Effect of Follower Forces on Aeroelastic Stability of Flexible Structures

A Thesis
Presented to
The Academic Faculty

by

Seungmook Chae

In Partial Fulfillment
of the Requirements for the Degree
Doctor of Philosophy

School of Aerospace Engineering
Georgia Institute of Technology
July 2004

Effect of Follower Forces on Aeroelastic Stability of Flexible Structures

Approved by:

Dewey H. Hodges, Committee Chair

Carlo Bottasso

Massimo Ruzzene

Anthony Hayter

Eugene L. Fleeman

Date Approved: July 7 2004

DEDICATION

To my wife

ACKNOWLEDGEMENTS

I would like to express my extreme gratitude to Dr. Dewey H. Hodges for his patient guidance during the past five years. Indeed, his ideas, attitude toward work, and everyday life have contributed to the way I look at life and work. Special thanks go to Dr. Mayuresh J. Patil for his assistance and training given to me while obtaining my Master of Science at Georgia Tech. He gave me much help for running the wing flutter case and helped me a lot academically.

I am also grateful to my thesis committee members: Dr. Massimo Ruzzene, Mr. Eugene L. Fleeman, Dr. Carlo Bottasso, and Dr. Anthony Hayter for taking time to read the thesis and giving me the valuable comments.

My sincere appreciation and thanks go to Mark Swanson, who has been a good mentor and friend for me to better understand America. Also, I am grateful to all of my colleagues at Georgia Tech including Jon Wallace, Bongjun Yang, Kwangtae Ha, Richard Cross and Rinfu Li. Special thanks go to Dr. Wenbin Yu who has showed a great friendship and sincere help.

I want to express my love and great gratitude to my wife (Kyongmi Yang), parents (Jeomdong Chae, Soonja Kim), and parents-in-law (Keunseung Yang, Insook Kim) for their love, encouragement, and support.

This work was supported by the U.S. Army Research Office under Grant 40448-EG of which the technical monitor was Dr. Gary L. Anderson. I sincerely appreciate the support.

TABLE OF CONTENTS

LIST OF TABLES

LIST OF FIGURES

NOMENCLATURE

a_i	inertial reference frame for a wing
b	undeformed beam cross-sectional frame when used in subscript or supercript, otherwise semi-chord
B	deformed beam cross-sectional frame
C	rotation matrix from b basis to B basis
C_o	rotation matrix from I basis to b basis
C^{bW}	rotation matrix from W to b basis
C^{WI}	rotation matrix from I to W basis
C_d	drag coefficient of a circular cylinder
d	missile diameter
$\frac{dN}{dx}$	distributive normal force along the missile body
e	$\frac{\overline{e}}{l}$
$\overline{e}$	mass offset at the cross-section of a wing
$EI_2,\ EI_3$	spanwise, edgewise bending stiffnesses, respectively
$e_1,\ e_2,\ e_3$	first, second, third column vector of identity matrix, respectively
F_B	cross-sectional force in the B basis
f_B	external force in the B basis
f_o	external force acting on the reference point
g	gravity

G	gravity potential
H_B	cross-sectional angular momentum in the B basis
H_o	angular momentum of missile reference point
$\hat{H}_o$	angular momentum of reference point at the ends of time interval
I	inertial basis
K	kinetic energy density per unit length
K_θ	tangential end thrust direction control parameter
l	beam length
M_B	cross-sectional moment in the B basis
m	mass per unit length
m_B	external moment in the B basis
m_o	external moment acting on the reference point
P_B	cross-sectional linear momentum in the B basis
P_o	linear momentum of missile reference point
$\hat{P}_o$	linear momentum of reference point at the ends of time interval
r_b	position from the missile body reference point
S	missile cross-sectional area
T	missile thrust magnitude
T^*	$\log_{10}(T/mg)$
t	time
$t_1,\ t_2$	fixed time at the time interval
U	strain energy density per unit length or free stream velocity
u_b	displacement of the points on missile reference line in the b basis

u_o	displacement of missile reference point in the I frame
v	$\frac{V}{b\omega_{\theta_1}}$
V	air speed for wing analysis
V_B	linear velocity at the missile reference line in the B basis
v_o	linear velocity at the missile reference line in the b basis
W	wind frame when used in superscript otherwise work done by external forces
$X_{a.c}$	location of aerodynamic center
$X_{c.m}$	location of center of mass
$X_{c.p}$	location of center of pressure
x_1	axial coordinate
x_o	location of the missile reference point
α	angle of attack at the reference point
$\overline{\alpha}$	angle of attack and sideslip angle column matrix at the reference point
β	sideslip angle at the reference point
γ	force strain in the B basis or ratio of fuselage drag over total drag
δ	virtual variation
$\overline{\delta A}$	virtual action at the ends of a beam and at the ends of a time interval
κ	moment strain in the B basis
η	ratio of the drag coefficient of a circular cylinder of finite length to that of a circular cylinder of infinite length
θ	a column matrix of Rodrigues parameters, from b to B basis
θ_w	a column matrix of Rodrigues parameters, from I to W basis
ξ_B	mass offset from the missile reference line

ξ	nondimensional elemental coordinate
σ	$\frac{\overline{\sigma}}{l}$
$\overline{\sigma}$	radius of gyration at a wing section
λ	$\frac{EI_2}{GJ}$
τ	nondimensional time
μ	$\frac{m}{\rho_\infty \pi b^2}$
ω_1	first bending natural frequency of a missile
ω_o	angular velocity of missile body in the b basis
ω_{θ_1}	first uncoupled torsional frequency of wing
Ω_B	angular velocity at the missile reference line in the B basis
Π	$u_b + \overline{\alpha}(x - x_o)$
ρ_∞	free stream air density
$\dot{}$	partial differentiation with respect to time
$'$	partial differentiation with respect to x_1
$\hat{}$	discrete boundary value either at the ends of beam
	or at the ends of time interval
$\tilde{}$	antisymmetric dual matrix operator
subscript f	variable values at the final time of time interval
subscript i	each element number
subscript o	missile reference point
subscript s	variable values at the starting time of time interval
superscript T	transpose of a vector or a matrix

SUMMARY

Missile bodies and wings are typical examples of structures that can be represented by beam models. Such structures, loaded by follower forces along with aerodynamics, exhibit the vehicle's aeroelastic instabilities. The current research integrates a nonlinear beam dynamics and unsteady aerodynamics to conduct aeroelastic studies of missile bodies and wings subjected to follower forces.

The structural formulations are based on a geometrically-exact, mixed finite element method. Slender-body theory and thin-airfoil theory are used for the missile aerodynamics, and two-dimensional finite-state unsteady aerodynamics is used for wing aerodynamics. The aeroelastic analyses are performed using time-marching scheme for the missile body stability, and eigenvalue analysis for the wing flutter, respectively.

Results from the time-marching formulation agree with published results for dynamic stability and show the development of limit cycle oscillations for disturbed flight near and above the critical thrust. Parametric studies of the aeroelastic behavior of specific flexible missile configurations are presented, including effects of flexibility on stability, limit-cycle amplitudes, and missile loads. The results do yield a significant interaction between the thrust, which is a follower force, and the aeroelastic stability.

Parametric studies based on the eigenvalue analysis for the wing flutter, show

that the predicted stability boundaries are very sensitive to the ratio of bending stiffness to torsional stiffness. The effect of thrust can be either stabilizing or destabilizing, depending on the value of this parameter. An assessment whether or not the magnitude of thrust needed to influence the flutter speed is practical is made for one configuration. The flutter speed is shown to change by 11% for this specific wing configuration.

CHAPTER I

INTRODUCTION

Aerospace structures are subjected to tangential follower forces or lateral follower forces produced by jet and rocket thrusts. Studies on follower forces have been performed under various topics. Many elastic systems loaded by follower forces have been studied and the literature associated with the study is now very extensive. Much of this work has focused on the stability of beams and shells subjected to various types of follower forces. However, the literature of follower forces associated with aeroelastic stability of structures is very rare, and little work on the subject has been published. Aerospace structures require a minimum weight because any unnecessary structural weight would mean an decrease of flight range and payload. Because of this minimum weight requirement, structures are generally very flexible. Such structures are sometimes exposed to the extremity of flight conditions to meet the mission requirements. Missile bodies and aircraft wings have engine thrusts that can be modeled as follower forces. Those thrusts along with aerodynamics are dominant factors in determining the flight stability, and the interaction between the two is poorly understood. Traditionally, at the preliminary design phase, designers have not paid much attention to the effects of engine thrusts on the aeroelastic stability of aircraft. Existing analytical tools are based on very simple models at best. So, the identifying process of such

instabilities has usually been performed after making prototypes. Such a process is expensive and time consuming.

As mentioned above, missile thrust is a kind of follower force, but its role related to aeroelastic stability has not been well known. Also the classification issues of the missile defense industry prevent the free access to the literature that might exist. Before discussing missile follower forces further, one needs to know what missiles experience during flight and what kind of problems have been solved or not solved. Missile development design has seen growing emphasis of higher speeds, more demanding maneuvers, and higher flexibility to meet various mission requirements. For example, several U.S. Army programs, such as extended range projectiles, the compact kinetic energy missile (CKEM) and the ARROW system require increased maneuverability and flexibility, thus leading to an increase of the relative importance of structural loads and deformation in the multidisciplinary problem.

Frequently missiles, rockets, and projectiles must deliver the last ounce of performance in order to meet their design objectives. For example, projectile designers strive to maximize the payload that the system delivers to a specified range; alternatively, they may strive for the maximum range for a given payload. Since very small relative changes in total mass may mean large relative changes in payload mass, even very small margins of gain are important. The extended range projectile program calls for the increase of payload mass by the use of composites in structural design. Defensive missiles, projectiles that are rocket powered in portions of their flight profiles (such as the CKEM), and smart missiles may be

designed to deliver precise hits with maximum final kinetic energy or velocity in order to effectively knock out an incoming missile, tank, or other enemy weapon. Greater sophistication in such areas as the evasive maneuvering capability of enemy weapon systems, for example, may require new generations of weapon system to deliver higher speeds and sustain higher loads and skin temperatures.

It is important to recognize the potential nonlinearities which can arise in both missiles and projectiles. One source of nonlinearities in missiles is a large axial force, so that even to get the standard linear equations one must linearize about a nontrivial state. Additional nonlinearities in both missiles and projectiles can arise due to free-play in threaded and snap joints. Also, fins on missiles and projectiles have nonlinearities due to large deflections and free-play in the hinges. Further nonlinear effects come about from matter shifting inside the casing. The need to account for imperfections and free-play effects further motivates the approach based on exact nonlinear kinematics.

Presently, missile conceptual designers specify the stiffness of the missile to structural designers. This specification without feedback and iteration does not facilitate multidisciplinary design optimization. Furthermore, even though the designs are driven by stiffness and not by strength, no attempt has been made until now to take advantage of the elastic couplings afforded by use of composites. Higher loads are likely to occur due to increased demands placed on modern equipment, and there is a higher probability of the occurrence of static and dynamic aeroelastic instabilities. Nevertheless, present methodologies are incapable of coping with these problems. Designers must wait until the prototype stage to

see whether or not there are going to be aeroelastic problems in the various flight regimes of the system. This approach is quite wasteful and inefficient.

The above observations also suggest coupling between the flight mechanics, guidance and control of a missile and its structural dynamics and aeroelasticity. A strictly optimal trajectory may induce higher internal loads and deformation, and aeroelastic phenomena can affect the originally planned missile trajectory. Present methodologies do not allow the exploration of this coupling. The stability problem due to thrust is a strictly dynamic stability issue, but aeroelastic phenomena may influence it. Unlike conventional flight vehicles, however, the static and dynamic aeroelastic instabilities may be coupled with flight dynamics modes. It is well known that a static criterion of stability is not sufficient in systems loaded by follower force such as thrust. Thus, a statically stable missile may be dynamically unstable. Structural deformation may affect the stability, and use of elastic tailoring may allow the designer to avoid aeroelastic instabilities in the design space early in the design effort.

Recent designs have emphasized the use of composite materials to keep the weight down. As the duration of flight and flight velocity are increased, the rise in casing temperature due to aerodynamic heating may become important. A significant rise in temperature may bring about a degradation in the stiffness properties of the composite materials, particularly in the matrix. The increased flexibility may enhance aeroelastic effects, creating non-negligible flexibility effects that interfere with the control system's ability to ensure that the missile or projectile reach precisely the desired destination.

With these trends in view, it seems imperative that modern analytical tools be created, so that a far better understanding of the influence of missile design parameters and operating conditions on their aeroelastic stability and loads can be obtained. Several issues introduced here will be discussed and their study conducted within one framework, in which the structural part is based on a mixed variational formulation which is geometrically exact and based on finite elements and aerodynamic theories which vary according to the flight regime and missile geometry. The motivations for specific aspects of the missile aeroelasticity study are well depicted in Fig. 1.

Aeroelasticity itself is a vast field with wing aeroelasticity having a large amount of literature. However, the role of wing engine thrust in aeroelastic stability has been neglected. The effect of thrust is modeled as a follower force of prescribed magnitude. Without the thrust force, the wing is easily shown to become unstable for freestream airspeeds greater than the flutter speed. On the other hand, in the absence of aerodynamic forces, the wing becomes unstable for values of the thrust in excess of a critical magnitude of the force. When both effects are present, the airspeed at which the instability occurs depends on the thrust magnitude. The effect of thrust can be either stabilizing or destabilizing, depending on the value of various parameters. So it would be a useful idea to find the stability boundary for the interaction of thrust and aerodynamic force.

The aim of the current research is to investigate the effects of follower forces on aeroelastic stability of both missile and aircraft. Missile aerodynamics is quite complex and analytical models cannot exactly simulate the complex flow under

various flight conditions. However, an aerodynamic model that is representative of some typical flight conditions is sufficient to see how aerodynamics interacts with thrust. As for the aircraft wing aerodynamics, a finite-state two-dimensional unsteady aerodynamic model is employed. Structural models for both missile and aircraft wing are based on the mixed variational formulation. It should be noted that most missile flutter problems shown in the literature have only to do with the missile fins. The research effort on missile body flutter has gone through some difficulty due to limited literature and thereby some validation is unlikely.

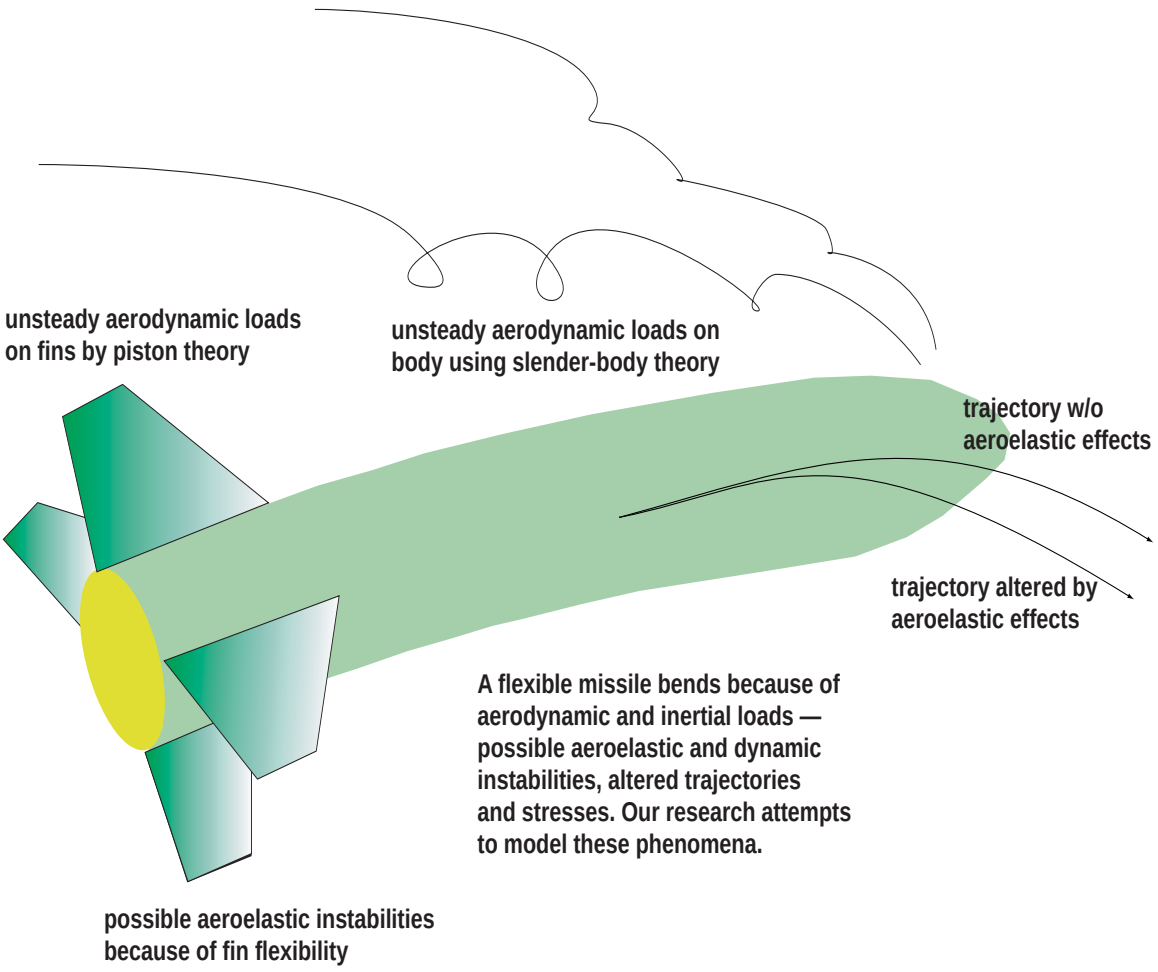

Fig. 1: Schematic of missile problem

CHAPTER II

LITERATURE SURVEY

In-flight missiles and projectiles experience various static, dynamic and aeroelastic stability issues with or without thrusts. But those problems have not had sufficient attention and there were at most a couple of published attempts to include the effects of aeroelasticity on the trajectory. Also, the flight mechanics of elastic missiles has seen little attention until recent years. Missiles and projectiles are typical examples of structures that can be represented by beam models. Indeed, several stability problems related to missiles have been solved mostly by linear beam analyses (Euler-Bernoulli or Timoshenko beam analysis, analytically or numerically). However, since those approaches are basically linear, they could not assess the nonlinear features arising from the structural dynamics or aeroelasticity. Integrated nonlinear tools that are capable of analysis of multidisciplinary problems such as those mentioned above do not yet exist.

As missiles and projectiles, aircraft wings are flown with high propulsion that can be modeled as a beam with lateral follower force. In the case of a high-thrust engine mounted on a flexible wing, the effects of the thrust on the flutter speed may be important, especially in the case of aircraft with very flexible wings. If there is any instability related to wing-mounted engine thrust, one needs to see which parameters are playing important roles.

In order to place the proposed work in the right perspective, a literature survey is undertaken and divided into four sections, which are stability problem due to thrust, static and dynamic aeroelastic instability, trajectory optimization, and finally flutter of wing mounted engine.

2.1 Stability Problem Due to Thrust

Beal [1] investigated the stability of a uniform free-free beam under a controlled follower force. For the case of a constant thrust without a directional control system ($K_\theta = 0$; tangential end thrust), he obtained the coalescence branches and the first critical thrust of flutter associated with beam bending. The Galerkin technique gave two zero eigenvalues for all values of thrust at $K_\theta = 0$. Beal concluded from physical reasoning that one eigenvalue was associated with a rigid-body translation mode, and the other with a rigid-body rotation accompanied by translation. So the system is neutrally stable a priori, no matter whether the vibratory modes are stable or not. But here the critical thrust is defined concerning bending vibratory modes. Beal showed that for the constant thrust with directional control, the critical thrust magnitude corresponds to a reduction of the lowest frequency to zero. Finally for the case of pulsating thrusts, he concluded that the longitudinal stiffness plays an important role by showing instabilities caused by the variations of the fundamental longitudinal beam frequency.

Peters and Wu [2] studied the lateral stability of a free-flying column subjected to an axial thrust with directional control. They concluded that under the

condition of no direction control of the follower force, a pair of zero eigenvalues exist for all forces with an eigenfunction of rank 1 corresponding to rigid-body translation and an eigenfunction of rank 2 corresponding to the rigid-body rotation. But the methods they employed are restricted to models where the rotation sensor is located at the end of the beam. The maximum stable thrust in those models is dependent upon sensor location. Wu [3] investigated the relation between the critical load and eigencurves by using a finite element method. He concluded that the magnitude and location of a concentrated mass can improve the stability characteristics of a missile. Park and Mote [4] studied a free-free Euler-Bernoulli beam, transporting a concentrated mass with rotary and transverse inertia under end thrust. Effects of axial location of the mass and the beam rotation sensor were investigated. For the case of no directional control, either flutter or divergence type instabilities may occur, depending on the magnitude and location of the concentrated mass. The location and the ratio of the concentrated mass to the total beam mass were calculated for force to be maximized. With directional control the instability first occurs with increasing force (called the primary instability). It can be either of the flutter or divergence type depending upon the rotation sensor location. Kirillov and Seyranian [5] performed a study on optimal distribution of mass and stiffness for a beam moving in space under a tangential end force. Their results showed that stability characteristics of the moving beam can be radically improved by using appropriate choices of mass and stiffness distributions. However, the analysis did not consider aerodynamics.

Park [6] studied dynamic stability of a free-free Timoshenko beam under a

controlled constant follower force. Unlike the above analyses, the effects of rotary inertia and shear deformation on the stability of the beam with a controlled follower force were investigated. In the case of no directional control, he concluded that the instability at the critical force is of flutter type and the critical force is increased as shear deformation parameter increases. With directional control, the primary instability is of either flutter or divergence type depending upon the rotation sensor location and the magnitude of the sensor gain. From a practical point of view, the effect of rotary inertia was negligible.

Because of difficulties in realizing a follower force in a laboratory setting, there has been little progress on finding the flutter limit experimentally. Sugiyama *et al.* [7] experimentally verified the effect of damping on the flutter of cantilevered column under rocket thrust and experiment was conducted by the direct installation of a solid rocket motor to the tip end of the columns.

Kim and Choo [8] investigated a Timoshenko beam subjected to a pulsating follower force, previously addressed only by Beal. The effects of axial location and translation inertia of the concentrated mass are studied, and the relationship between critical forces and widths of instability regions in the vicinity of $2\omega_1$ (twice the first natural frequency of bending vibration) are also examined. They concluded that the variation of the instability region near $2\omega_1$ is closely related to the type of critical force.

It is well known that spinning has a stabilization effect against the directional change of the spinning axis. In a rigid body the stabilization characteristics vary as the spinning speed is increased. However, in case of a flexible beam model, the

stability region may vary due to the effects of elastic modes. Yoon and Kim [9] analyzed the dynamic stability of a spinning beam subjected to a pulsating thrust. They concluded that the critical load of a free-free beam under constant thrust was not affected by spinning motion, but as the spinning speed was increased, the instability regions were reduced.

Leipholz and Piche [10] studied the effect of self-weight and follower forces on the stability of elastic rods using the two-term Galerkin method. Their study included pinned-pinned rod, clamped-free rod, and free-free rod. They argued that a point mass approximation could not lead to divergence and critical flutter loads, and such a problem could be avoided by assuming that the mass distribution is strictly positive along the entire length of the rod.

2.2 Static and Dynamic Aeroelastic Instability

Linear flight mechanics of spinning projectiles dates back to early 20th century and was extended after World War II, see for example, Refs. [11, 12, 13] and Platus [14] reformulated these results in missile-fixed coordinates for reentry vehicles. Later, nonlinear flight mechanics was extensively addressed in Refs. [15, 16, 17, 18, 19, 20]. Nonlinear flight mechanics of flying missiles still holds an important place in identifying various in-flight problems.

When we refer to missile aeroelasticity in the literature, more literature has been concerned with missile fins than the missile body itself since missile fins are more flexible and movable and thereby more likely to be in a condition of flutter before a missile body instability. For more discussion, Refs. [21, 22, 23, 24] deal

with the aeroelastic behavior of missile fins.

For increasingly flexible missiles there is an increasingly important coupling between so-called flight dynamics phenomena and aeroelasticity. For example, Matejka [25] conducted both analytical studies and wind tunnel tests of a two stage Terrier-Tomahawk 9 rocket vehicle. Aeroelastic bending (or more specifically, the adverse movement of the system center of pressure due to vehicle flexibility) explains an observed severe reduction in the stability, rendering the rigid-body static stability criteria insufficient. Both the results of the analytical procedure and the wind tunnel tests verified that it was possible for the flexible flight vehicle to be in a condition of roll resonance during powered flight, while highly stable flight is predicted based on rigid-body considerations.

Moreover, Elyada [26] studied the aeroelastic divergence of a rocket vehicle in closed form, where roll resonance and trajectory errors can be predicted. Assuming that the accelerations associated with deformation are negligible compared to the ones connected with rigid-body motion, general divergence analyses are considerably simplified. He showed that the short-period mode angular frequency is always less than that of the associated rigid vehicle. In a vehicle designed to roll at a frequency smaller than its rigid short period mode angular frequency, failure to consider this may result in an unexpected roll resonance. In aerodynamically misaligned vehicles, moderating nonlinear effects or structural failure must occur at substantially lower dynamic pressures.

There are two kinds of misalignment in a missile. One is aerodynamical and the other is thrust. Nakano [27] conducted study on the bending load due

to thrust misalignment. Body divergence, regarded as a phenomenon where the aeroelastic equilibirium without stabilizing moment is lost, was analyzed in terms of dynamic pressure and load factor. He assumed steady-flow aerodynamics and a straight beam for the body, and showed the relation between loads and misalignment values. He concluded that in unguided missiles, the ratio of flight dynamic pressure over divergence dynamic pressure should be kept far below unity because of prediction uncertainty of aeroelastic parameters or performances and load due to wind.

Crimi [28] derived from Lagrange's equations the linear equations of motion for a spinning, aeroelastic missile but structural damping was not included in the formulation. He showed that divergence and dynamic stability are functions of velocity, spin rate and bending stiffness, and that aeroelastic effects cause degradation of vehicle static longitudinal stability as bending stiffness is decreased. Platus [29] derived a nonlinear equation of motion of slender, spinning missiles using a Lagrangian approach. He obtained nonlinear terms that produce nonlinear coupling between the elastic deflections and the rigid-body motions. However, no attempt was made to assess the relative importance of the nonlinear terms. He showed that missile flexibility has an effect on static stability and reduces the critical frequency for pitch-roll coupling. Also, viscous structural damping has a destabilizing effect on stability at roll rates above the critical frequency for roll-pitch coupling. One should be able to predict the spin and deflection history at any time in flight for a given projectile under given flight conditions. Stearns *et*

al. [30] provides such results, but details of his analysis and model are not available for verification or review. Legner *et al.* [31] studied the primary effects of segmentation (which is used for enhancing the penetrating characteristics of the projectile) and flexure on hypervelocity projectiles, but the details of his analysis are also unavailable. They showed effect of bending frequency on angle of attack and displacement of the projectile tip. They concluded that the most significant tip displacement corresponds to regions in time when the angle of attack is maximum, and that increase of bending frequency leads to an increase of angle of attack. Livshits *et al.* [32] studied dynamic aeroelastic analysis of free flight rockets, incorporating effects of follower forces together with imperfection factors (dynamic imbalance, thrust misalignment and nonlinear fittings) excluding only gyroscopic effects, which are typical to spin-stabilized type of rockets only. All the loads acting on the rocket were considered as follower forces, including the centrifugal forces coupled with the rocket bending. They showed the resonance type of instability; *i.e.*, when the spin rate crosses the rocket's fundamental frequency in bending, the rocket continues to accelerate in roll, developing growing angles of attack after the burnout. They also demonstrated the importance of the imperfections, especially the dynamic imbalance and thrust misalignment.

Even though structural dynamics of flying missiles is essential in getting structural design requirements leading to high performance, it has not been dealt with much in the literature in comparison with its importance. The range of missile stiffness should be known at the preliminary design phase for optimum design in terms of maneuverability and stability. Maloney *et al.* [33] made an extensive

study of mechanical joints in common use and investigated their effects on the flight modes and stiffness. They concluded that tactical missile joints play a major role in dissipating vibratory energy and the energy dissipation comes from both sliding friction and gas pumping.

Some evidence shows that long finned missiles such as some anti-tank kinetic energy projectiles have been forced to spin at rates close to their lowest elastic frequency and have been subject to large inelastic deformations. Special solutions showing spin lock-in at the lowest elastic frequency were developed by Mikhail [34] and Murphy and Mermagen [35]. Mikhail showed examples of spin lock-in when fin damage produces a roll inducing moment sufficient to cause a steady-state spin greater than the lowest elastic frequency. Murphy and Mermagen [36] insisted that his results should be dismissed due to incorrect expressions for the angular momentum. Murphy and Mermagen [35] approximated the elastic missile by three rigid bodies connected by two massless elastic beams and showed that it is impossible to cause spin lock-in by roll inducing moment and zero initial spin alone. But the use of the three-body model is a major simplification of the actual physical problem. Later they replaced three body model with continuous elastic model using differential equations in Ref. [36] and obtained numerical results for the natural frequencies, flexing waveforms and equilibrium spins for a specific missile.

Reis and Sundberg [37] investigated the causes of large coning angle that a Nike-Tomahawk sounding rocket experienced during flight. They assumed that Magnus forces, aeroelastic bending, and/or lee-side boundary separation were

probable reasons. Based on flight data they showed that aeroelastic bending was one of the causes. Cochran and Christensen [38] studied the post-launch effect of transverse bending of a spinning free-flight rocket during the guidance phase. They used two different methods which are a simple two-body model and a sophisticated assumed-modes model.

2.3 Trajectory Optimization

The optimal trajectory is usually found by minimizing a performance index that contains constraints on state and control variables as well as a minimum time structure, and is based on a point mass model. The simplistic models that are often used are unable to capture coupling between optimal trajectories and the stability and loads that can be provided by powerful simulation programs using a full 3-D finite element method. Nasuti and Innocenti [39] included maneuverability and agility considerations in the optimization process, with a kinematic model and constraints obtained from dynamic limits. A maneuver envelope was proposed that would allow the incorporation of design parameters into agility optimization. The speed from propulsive considerations, the load factor from structural limitations, turn rate from stall characteristics were bounded from the maneuverability envelope. Another constraint was an estimated upper bound on turn rate in post-stall condition function of the maximum propulsive control.

Muzumdar and Hull [40] developed an optimal midcourse guidance law for a high-thrust, bank-to-turn, short-range attack missiles. The analytical guidance law obtained by making approximations in the optimal control problem works

for midcourse guidance but needs terminal guidance to hit the target. The error compensation (EC) guidance law enables the missile to hit the target without terminal guidance. The EC guidance law is obtained by replacing the approximation terms by bounded controls, where the bounds are handled indirectly by adding penalty terms to the performance index. The EC weights are determined by using the EC control in the trajectory optimization problem and minimizing the flight time with respect to the weights.

Wang *et al.* [41] developed an optimality-based feedback trajectory shaping guidance law. The guidance law is assumed to be in some feedback form. The optimal solution involves solving a nonlinear two-point, boundary-value problem, which is formidable and expensive. A common practice is to parameterize the control and solve a suboptimal control problem through parameter optimization. The approach combines the design of guidance parameters and control gains into the optimization process. It was shown that this control law would achieve better performance and be robust with respect to the initial condition perturbations although the open loop control has the shortcoming that control is less responsive to the perturbations.

Hallman [42] studied how the optimal solution is affected by changes to design parameters that are held fixed during the optimization, after determining an optimum trajectory design. This area of study is called postoptimality or sensitivity analysis. As opposed to the conventional brute force approach where repeated optimization problems are solved, sensitivity analysis allows an efficient, accurate, and systematic methodology for studying perturbations about an optimal

design.

Han and Balakrishnan [43] investigated the use of an "adaptive critic" controller to steer an agile missile to completely reverse its flight path angle in minimum time starting from given initial and final Mach numbers and with a constraint on the minimum flight Mach number. This was undertaken for optimal solutions that encompass perturbations to the assumed initial conditions or a family of initial conditions. The neighboring optimal control allows pointwise solutions of an optimal two-point, boundary-value problem to be used with a linearized approximation over a range of initial conditions but can fail outside the regime in which linearization is valid. Dynamic programming can handle a family of initial conditions for linear as well as nonlinear problems. Both solution methods are computationally intensive, and the solution is not available in feedback form. For implementation this becomes a drawback. Outside of dynamic programming, there is no unified mathematical formalism under which a controller can be designed for nonlinear systems. They proposed a formulation that (1) solves a nonlinear control problem directly without any approximation to the system model, (2) yields a control law in a feedback from as a function of the current states, and (3) maintains the same structure regardless of the type or problem. Such a formulation is afforded by the field of neural networks, specifically, the adaptive critic architecture. They showed that this method provides optimal control to the missile from an envelope of initial Mach numbers in minimum time. An added advantage in using these neurocontrollers is that they provide minimum time solutions even when one changes the initial flight path

angle from zero to any nonzero (positive) value. There has been no one tool for such solutions except for dynamic programming.

Imado *et al.* [44] studied optimal midcourse guidance laws for medium-range, air-to-air missiles that employ different guidance modes depending on the required missile velocity and navigation time. This was done for two separate problems: (1) against a faraway or low-altitude target where missile velocity is a prime factor, so that the midcourse guidance law that maximizes the residual velocity is preferable; (2) against a near target where the time margin is most important so that the midcourse guidance law that minimizes the interception time is preferable. After the required missile residual velocity is analyzed against a conventional and an advanced target, four types of midcourse guidance laws depending on objectives are presented, each with its merits and demerits.

2.4 Flutter of Wing Mounted Engine

Flutter of flexible structures due to aerodynamic effects is an old and practical problem, and many papers and books have been written about various aspects of it. See for example, Refs. [45, 46, 47]. It is also well known that follower forces can induce flutter. The well-known Beck problem [48], a cantilever beam excited by an axially compressive follower force, is a commonly analyzed problem in the literature. Indeed, there are now quite a few papers and a few books devoted to the stability of flexible structures loaded by follower forces. See, for example, Refs. [49, 50, 51] for cantilever beams and Refs. [6, 8, 52] regarding the stability of a free-free beam subjected to a follower force.

In spite of the huge body of literature on the aeroelasticity of lifting surfaces, there is very limited literature concerning the effects of the thrust of a wing-mounted engine on aeroelastic flutter. Indeed, in contrast to the significant number of papers that deal with various aspects of Beck's problem (cantilevered beam loaded by an axial follower force), the problem of a cantilevered beam excited by a *transverse* follower force has not received much attention in the literature. This type of system was first considered in a stability analysis by Como [53].By assuming a rigid body with specified mass and moments of inertia attached to the tip and neglecting the distributed mass of the beam, he obtained an analytical value for critical load. Wohlhart [54] extended Como's work to include the distributed mass and allowed the position of the added mass, moments of inertia, and the follower force (all at the same point) to vary. This excellent paper presents an extensive parametric study, taking into account all relevant parameters.

Restricting the location of the force and rigid body to the free end, Feldt and Herrmann [55] investigated the flutter instability of a wing subjected to the transverse follower force in the presence of airflow. Therein it was reported that an increase in tip mass always stabilizes the system, but according to Ref. [54] this is not always true if one considers only the thrust-induced flutter. They considered only one value of the ratio of bending stiffness to torsional stiffness in their study, a value for which thrust is destabilizing. Moreover, the thrust-induced flutter results presented by Ref. [55] do not agree with those of Ref. [54].

CHAPTER III

PRESENT WORK

The ideas embedded in the introduction along with all the works in the literature survey could be explored within one framework which consists of structural formulation and aerodynamic model. This work will be conducted in parallel for both missile body aeroelasticity and the stability of aircraft wing thrust. The structural part is basically the same for the both systems and based on the mixed variational formulation. The differences are that in case of missile flutter, the rigid-body variables are not given but varying in a time-marching scheme to consider the rigid-body motion. The missile body analysis is based on time-marching, but eigenvalue analysis is conducted for wing flutter. This finite-element based nonlinear one-dimensional analysis for the structural formulation is very powerful in that it is geometrically exact and allows the use of very simple shape functions. The most challenging part for the missile comes from the aerodynamics which is very dependent on the geometry and flight conditions. However, the present approach to the missile aerodynamics is to build a representative aerodynamic model suited to serve the current research purposes at the potential sacrifice of some accuracy. Thus, analytical, closed-form aerodynamic expressions or at least less computational methods, such as a modified Newtonian method and piston

theory, are preferred. Another thing to be said about missile aerodynamics expressions is that differentiated variables should be expressed in other kinematic variables in keeping with the lowest order of differentiations in the structural formulation. For the wing flutter problem, aerodynamic forces are calculated using a finite-state, two-dimensional unsteady aerodynamic model. Each follower force of missile thrust and wing engine thrust can lead to instabilities without considering aeroelasticity, and the same applies to only aeroelasticity. Therefore, the interactions of follower forces and aerodynamic forces make one think of the possible stability boundaries suggested by Leipholz [50] and Huseyin [56]. From the following chapters, respective stability boundary will be explored.

CHAPTER IV

EFFECT OF THRUST ON MISSILE BODY STABILITY

Many authors have revealed there are two zero eigenvalues in free-free beam problems with a follower force. The eigenvalues refer to two rigid-body modes, thus a free-free beam is a priori only neutrally stable in these two rigid-body modes. This does not involve bending of the beam structure. Here the stability analysis is only concerned with bending modes.

Missile flight can be divided into two phases, powered flight and free flight without thrust. During the powered portion of the flight, loads and dynamic stability are the main issues. Projectiles are under severe stresses. Total mass varies from propellant consumption and the aerodynamic center changes as well due to possible bending deformation from considerable lift on both nose and tail and the variation of aerodynamic coefficients. There is a certain velocity where the shifted location of the aerodynamic center coincides with the location of the center of mass. But this situation can be avoided by keeping the burnout velocity below the velocity. Such a variation trend that is depicted in Ref. [57] is introduced for clarification in Fig. 2 for the movement of missile center of mass and aerodynamic center for both the rigid- and the flexible-body models as a function of velocity.

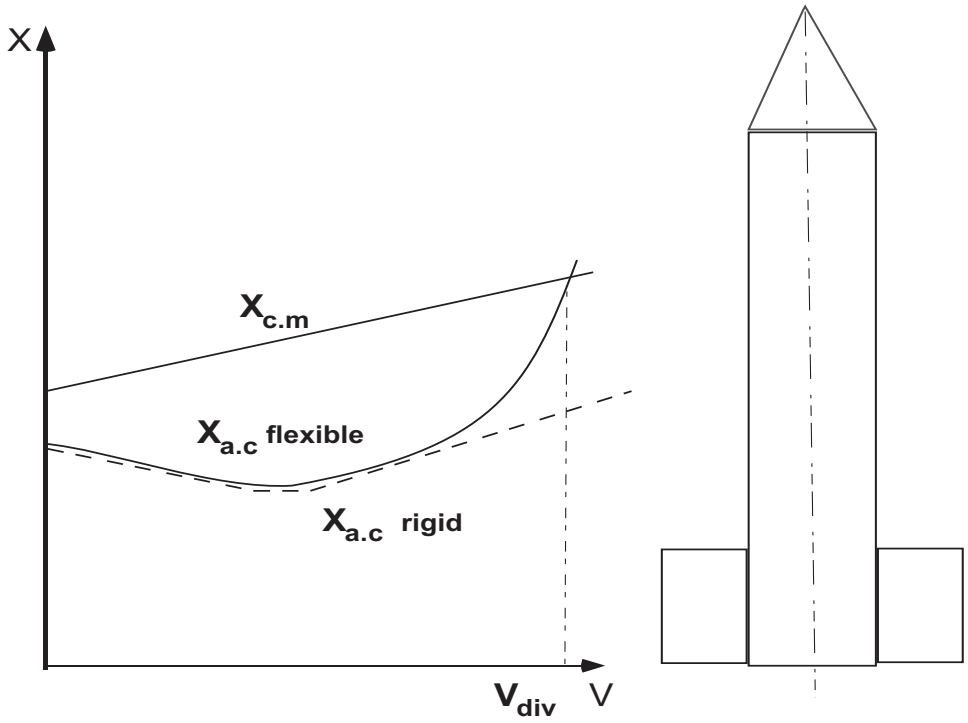

Fig. 2: Typical movement of the center of mass and aerodynamic center

During the powered flight, the missile reaches the maximum speed, the so-called burnout velocity. After the burnout velocity, the missile decelerates. Therefore, accelerating flight with thrust, steady flight when the thrust magnitude is equal to drag, and coasting or ballistic flight without thrust are of interest to current research efforts.

4.1 Structural Formulation

The structural part of the formulation comes from the mixed variational formulation based on the exact intrinsic equations for dynamics of moving beams [58].

The modifications to the original variational principle are the inclusion of the gravitational potential energy and appropriate energy variation for dealing with rigid-body dynamics, the analysis of which is needed for the missile time-marching scheme. The frames presented here are the undeformed beam cross-sectional frame (the b basis), the deformed cross-sectional frame (the B basis), and the inertial frame (the i basis). Here we follow the same rule for the variable notation as shown in Ref. [58], except that the subscript o represents the missile reference point for denoting rigid-body motion. The variables with subscript b and o are measured in the b frame, except for u_o, the basis for which is that of the inertial frame. The variational formulation starts with extended Hamilton's principle

$$\int_{t_1}^{t_2} \int_0^l \left[\delta(K-U) + \overline{\delta W}\right] dx_1\, dt = \overline{\delta \mathrm{A}} \tag{1}$$

where t_1 and t_2 specify the time interval over which the solution is sought; K and U are the kinetic and strain energy densities per unit length, respectively; and $\overline{\delta \mathrm{A}}$ is the virtual action at the ends of the beam and at the ends of the time interval. The contribution of all gravitational forces is handled by means of its potential energy, which is written as

$$G = \int_0^\ell mge_3^T[u_o + C_o^T(r_b + u_b + C^T\xi_B)]dx_1 \tag{2}$$

where the superscript T indicates the transpose of vector or matrix, e_3 is $[0\ 0\ 1]^T$, r_b is the position from the missile body reference point, u_o is the displacement of missile reference point in the i frame, u_b is the displacement of the points on missile reference line in the b frame, ξ_B is the mass offset from the missile reference line, m is mass per unit length, C_o is the rotation matrix from i frame

to b frame, and C is the rotation matrix from b frame to B frame. The kinematic relationships and the expressions for the velocities and the generalized strains can be written as

$$v_o = C_o \dot{u}_o \tag{3}$$

$$\widetilde{\omega}_o = -\dot{C}_o C_o^T \tag{4}$$

$$V_B = C\left[v_o + \dot{u}_b + \widetilde{\omega}_o(r_b + u_b)\right] \tag{5}$$

$$\Omega_B = \left(\frac{\Delta - \frac{\widetilde{\theta}}{2}}{1 + \frac{\theta^T\theta}{4}}\right)\dot{\theta} + C\omega_o \tag{6}$$

$$\gamma = C(e_1 + u_b') - e_1 \tag{7}$$

$$\kappa = \left(\frac{\Delta - \frac{\widetilde{\theta}}{2}}{1 + \frac{\theta^T\theta}{4}}\right)\theta' \tag{8}$$

where the $\widetilde{(\ )}$ operator converts a 3×1 column matrix, say $v = \lfloor v_1 \quad v_2 \quad v_3 \rfloor^T$, to its 3×3 antisymmetric dual matrix

$$\widetilde{v} = \begin{bmatrix} 0 & -v_3 & v_2 \\ v_3 & 0 & -v_1 \\ -v_2 & v_1 & 0 \end{bmatrix} \tag{9}$$

$e_1 = \lfloor 1 \quad 0 \quad 0 \rfloor^T$, $\dot{(\ )}$ and $(\ )'$ are differentiations with respect to time and x_1, respectively. The orientation of the B frame with respect to the b frame is represented using Rodrigues parameters, which have been applied to nonlinear beam problems with success. The rotation matrix relating the B frame to the b frame is written as

$$C = \frac{\left(1 - \frac{1}{4}\theta^T\theta\right)\Delta - \widetilde{\theta} + \frac{1}{2}\theta\theta^T}{1 + \frac{1}{4}\theta^T\theta} \tag{10}$$

where θ is the rotational displacement of the points on missile reference line in the b frame. For the orientation of the missile body frame (i.e. the b frame), however, the regular use of the Rodrigues parameters is insufficient because of their well-known singularity at a rotation angle of 180°. Thus, the direction cosines of b in i are used as rotational variables for the rigid-body motion of the missile. The strain and force measures, along with velocity and momentum measures, are related through the constitutive laws in the form

$$\begin{Bmatrix} P_B \\ H_B \end{Bmatrix} = \begin{bmatrix} m\Delta & -m\widetilde{\xi}_B \\ m\widetilde{\xi}_B & I \end{bmatrix} \begin{Bmatrix} V_B \\ \Omega_B \end{Bmatrix}$$
$$\begin{Bmatrix} F_B \\ M_B \end{Bmatrix} = [S] \begin{Bmatrix} \gamma \\ \kappa \end{Bmatrix} \tag{11}$$

All the elastic virtual variations are the same as the expressions in [58] except for the virtual quantities related to rigid-body variables. Here the details of the rigid-body part are described. After some manipulations, the virtual variations of rigid-body variables v_o and ω_o in Eqs. (3) and (4) may be expressed as

$$\delta v_o = \delta\dot{q}_o + \widetilde{\omega}_o\delta q_o + \widetilde{v}_o\delta\psi_o \tag{12}$$

$$\delta\omega_o = \delta\dot{\psi}_o + \widetilde{\omega}_o\delta\psi_o \tag{13}$$

where δq_o and $\delta\psi_o$ are virtual quantities defined in the b frame, *i.e.* $\delta q_o = C_o \delta u_o$. Detailed derivations are provided in Appendix A.1 and A.2. Also, Eq. (2) can be expressed as

$$\begin{aligned}\delta G =& \delta q_o^T C_o \int_0^\ell mge_3 dx_1 - \delta\psi_o^T \widetilde{C_o e_3} \int_0^\ell mg(r_b + u_b + C^T \xi_B) dx_1 \\ &+ \int_0^\ell \overline{\delta q}_B^T C C_o e_3 mg dx_1 + \int_0^\ell \overline{\delta\psi}_B^T \widetilde{\xi_B} C C_o e_3 mg dx_1\end{aligned} \tag{14}$$

A complete derivation for this expression is given in Appendix A.3. Adding the varying action and virtual work terms contributed by the rigid-body variables, one finds that

$$\overline{\delta \mathrm{A}}_o = (\delta q_o^T \hat{P}_o + \delta\psi_o^T \hat{H}_o)\Big|_{t_1}^{t_2} \tag{15}$$

$$\overline{\delta W}_o = \delta q_o^T f_o + \delta\psi_o^T m_o \tag{16}$$

where f_o and m_o are column matrices containing the measure numbers of force and moment vectors acting on the reference point in the b frame; $\hat{P}_o$ and $\hat{H}_o$ are linear and angular momenta of reference point at the ends of specified time interval in the b frame. Additional terms of elastic virtual quantities stemming from rigid-body variations are

$$\delta V_B^T : \delta v_o^T C^T + \delta\omega_o^T (\widetilde{r}_b + \widetilde{u}_b) C^T \tag{17}$$

$$\delta \Omega_B^T : \delta\omega_o^T C^T \tag{18}$$

For the variations of individual energies, and virtual work done on the system, we have

$$\delta K = \delta v_o^T P_o + \delta \omega_o^T H_o + \int_0^l (\delta V_B^T P_B + \delta \Omega_B^T H_B) dx_1 \tag{19}$$

$$\delta U = \delta G + \int_0^l (\delta \gamma^T F_B + \delta \kappa^T M_B) dx_1 \tag{20}$$

$$\overline{\delta W} = \delta q_o^T f_o + \delta \psi_o^T m_o + \int_0^l (\overline{\delta q}_B^T f_B + \overline{\delta \psi}_B^T m_B) dx_1 \tag{21}$$

where the unknowns are F_B and M_B, the sectional force and moment measures in the B basis, respectively; P_B and H_B, the sectional linear and angular momentum measures in the B basis, respectively; γ and κ, the force and moment strains, respectively; V_B and Ω_B, the linear and angular velocity measures of the beam reference line in the B basis, respectively; and f_B and m_B, the external force and moment, respectively.

The expressions for various virtual quantities such as δV_B, $\delta \Omega_B$, $\delta \gamma$, and $\delta \kappa$ are substituted into the energy equations. In the mixed variational formulation, the appropriate kinematical and constitutive relations are enforced as additional constraints using Lagrange multipliers and are then adjoined to Hamilton's weak principle expressed in terms of given energies.

The modified weak form from the original mixed variational formulation including the rigid-body part in the proper way then can be written as

$$
\begin{aligned}
&\int_{t_1}^{t_2}\int_0^{\ell}\Bigg\{\left[\overline{\delta q}_B'^T-\overline{\delta q}_B^T\widetilde{\kappa}-\overline{\delta\psi}_B^T(\widetilde{e}_1+\widetilde{\gamma})\right]F_B+\left(\overline{\delta\psi}_B'^T-\overline{\delta\psi}_B^T\widetilde{\kappa}\right)M_B\\
&\quad-\Bigg[\dot{\overline{\delta q}}_B^T-\overline{\delta q}_B^T\widetilde{\Omega}_B-\overline{\delta\psi}^T\widetilde{V}_B+\delta v_o^TC^T\\
&\quad+\delta\omega_o^T(\widetilde{r}_b+\widetilde{u}_b)C^T\Bigg]P_B-\left(\dot{\overline{\delta\psi}}_B^T-\overline{\delta\psi}\widetilde{\Omega}_B+\delta\omega_o^TC^T\right)H_B\\
&\quad+\overline{\delta F}^T\left[e_1-C^T(e_1+\gamma)\right]-\overline{\delta F}'^Tu_b\\
&\quad-\overline{\delta M}^T\left(\Delta+\frac{1}{2}\widetilde{\theta}+\frac{1}{4}\theta\theta^T\right)\kappa-\overline{\delta M}'^T\theta\\
&\quad-\overline{\delta P}^T\left[v_o+\widetilde{\omega}_o(r_o+u_b)-C^TV_B\right]+\dot{\overline{\delta P}}^Tu_b\\
&\quad-\overline{\delta H}^T\left(\Delta+\frac{1}{2}\widetilde{\theta}+\frac{1}{4}\theta\theta^T\right)(C\omega-\Omega_B)\\
&\quad+\dot{\overline{\delta H}}^T\theta-\overline{\delta q}_B^Tf_B-\overline{\delta\psi}_B^Tm_B\Bigg\}dx_1dt\\
&\quad+\int_{t_1}^{t_2}\left(\delta G^*-\delta v_o^{*^T}P_o-\delta\omega_o^{*^T}H_o-\delta q_o^Tf_o-\delta\psi_o^Tm_o\right)dt\\
&=-\int_0^{\ell}\left(\overline{\delta q}_B^T\hat{P}_B+\overline{\delta\psi}_B\hat{H}_B-\overline{\delta P}^T\hat{u}_b-\overline{\delta H}^T\hat{\theta}\right)\Bigg|_{t_1}^{t_2}dx_1\\
&\quad+\int_{t_1}^{t_2}\left(\overline{\delta q}^T\hat{F}_B+\overline{\delta\psi}^T\hat{M}_B-\overline{\delta F}^T\hat{u}-\overline{\delta M}^T\hat{\theta}\right)\Bigg|_0^{\ell}dt-\left(\delta q_o^T\hat{P}_o+\delta\psi_o^T\hat{H}_o\right)\Bigg|_{t_1}^{t_2}
\end{aligned}
\tag{22}
$$

where algebraic expressions defining certain variables in terms of displacement and rotation variables are denoted by $(\,)^*$ and $(\,\hat{}\,)$ represents discrete boundary values either at the ends of beam or at the ends of time interval. In addition to the above formulation, Poisson equation ($\dot{C}_o+\widetilde{\omega}_oC_o=0$) of direction cosine matrix is adjoined using Lagrange multipliers, which is not included here for the

sake of brevity.

4.2 Aerodynamics

Available aerodynamics tools have been evaluated for computation of loads on missiles. Missile loads are very dependent on the flight condition and missile geometry. Several technical methods are extensively described in [59], [60], and [61]. The validity of slender-body theory, which is based on potential flow, has been well established by comparison with experimental data in [62] for a wide range of Mach numbers. An extended slender-body theory is discussed by [63]. An unsteady version of slender-body theory for aeroelasticity was presented in [47]. For our purposes, the aerodynamic loads on a missile body can be calculated with sufficient accuracy for the sort of interdisciplinary tradeoff studies we anticipate doing by using slender-body theory augmented by a viscous cross-flow theory; see [64]. There are parts of the missile for which these methods are not suitable, and for these other methods are used. For example, the loads on the missile fins and tail are calculated by thin-airfoil theory in low-speed flight and by piston theory [65] in hypersonic flight. With the combination of the viscous cross-flow theory of [64] and the potential flow slender-body theory in [47], we can take into account the bending deformation and unsteadiness of the flow. The resulting equation then reduces to

$$\begin{aligned}\frac{dN}{dx} = &-\rho_\infty \frac{dS}{dx}\left(U^2\frac{\partial \Pi}{\partial x} + U\frac{\partial \Pi}{\partial t}\right) + \eta c_d d\frac{\rho_\infty U^2}{2}\alpha^2 \\ &-\rho_\infty S\left(U^2\frac{\partial^2 \Pi}{\partial x^2} + 2U\frac{\partial^2 \Pi}{\partial x \partial t} + \frac{\partial^2 \Pi}{\partial t^2}\right)\end{aligned} \tag{23}$$

where $\Pi = u_b + \overline{\alpha}(x - x_o)$; N is the normal force column matrix; U and ρ_∞ are the freestream velocity and air density, respectively; $\overline{\alpha}$ is the angle of attack and sideslip angle column matrix at the reference point; x_o is the location of the reference point; η is the ratio of the drag coefficient of a circular cylinder of finite length to that of a circular cylinder of infinite length; c_d is the drag coefficient of a circular cylinder, and d and S are the missile diameter and the missile cross-sectional area, respectively. Since the aerodynamic forces involve higher derivatives, which do not allow one to use low order shape functions, the weak form including the aerodynamic forces in Eq. (23) needs to be integrated by parts to reduce the order of differentiation. Unfortunately, even after this integration by parts, there are still some derivatives of variables. Therefore, in accordance with the lowest order of differentiation for the variables in the expressions for aerodynamic forces, kinematic expressions such as

$$\dot{u}_b = (\Delta + \tilde{\theta})V_B - v_o - \tilde{\omega}_o(r_b + u_b) \tag{24}$$

$$u_b' = (\Delta - \tilde{\theta})(e_1 + \gamma) - e_1 \tag{25}$$

$$\dot{u}_2' = e_3^T(\Omega_B - C\omega_o) \tag{26}$$

$$\dot{u}_3' = -e_2^T(\Omega_B - C\omega_o) \tag{27}$$

$$U = \sqrt{v_o^T v_o} \tag{28}$$

are used to reduce the order of the derivatives. So, for differentiated Π,

$$\frac{\partial \Pi}{\partial x} = \begin{Bmatrix} 0 \\ u_2' + \beta \\ u_3' + \alpha \end{Bmatrix}$$

$$\frac{\partial \Pi}{\partial t} = \begin{Bmatrix} 0 \\ \dot{u}_2 + \dot{\beta}(x - x_0) \\ \dot{u}_3 + \dot{\alpha}(x - x_0) \end{Bmatrix}$$

In order to completely determine the angle of attack and sideslip angle quantities in terms of other kinematic quantities, we need to obtain the rotation matrix from the inertial frame to the wind frame, C^{WI}. From the frame definitions,

$$\begin{Bmatrix} q_1 \\ q_2 \\ q_3 \end{Bmatrix} = \begin{Bmatrix} C_{11}^{WI} \\ C_{12}^{WI} \\ C_{13}^{WI} \end{Bmatrix} = \frac{\Delta}{U} C_o^T v_o \tag{29}$$

If θ_w is defined as a column matrix of Rodrigues parameters, we can obtain

$$\theta_w = \theta_{w1} e_1 + \frac{1}{1 + q_1} [2\widetilde{e_1} + \theta_{w1}(\Delta - e_1 e_1^T)] C^{IW} e_1 \tag{30}$$

as given by [58]. After a holonomic constraint, θ_{w1}=0 is imposed, we obtain

$$\theta_w = \frac{2}{1 + q_1} \begin{Bmatrix} 0 \\ -q_3 \\ q_2 \end{Bmatrix} \tag{31}$$

so that

$$\begin{Bmatrix} \dot{q}_1 \\ \dot{q}_2 \\ \dot{q}_3 \end{Bmatrix} = \frac{\Delta}{U^2} [\{C_o^T \tilde{\omega}_o v_o + C_o^T a\} U - \frac{C_o^T v_o v_o^T a}{U}] \tag{32}$$

and

$$\dot{\theta}_w = \frac{2}{(1+q_1)^2}\begin{bmatrix} 0 \\ -\dot{q}_3(1+q_1)+q_3\dot{q}_1 \\ \dot{q}_2(1+q_1)-q_2\dot{q}_1 \end{bmatrix} \tag{33}$$

Thus, if one can get the one row components of rotation matrix C^{WI} from Eq. (29), rotation matrix C^{WI} and angular velocity of wind frame with respect to inertial frame can be determined as follows

$$C^{WI} = \frac{\left(1-\frac{1}{4}\theta_w^T\theta_w\right)\Delta - \widetilde{\theta_w} + \frac{1}{2}\theta_w\theta_w^T}{1+\frac{1}{4}\theta_w^T\theta_w} \tag{34}$$

$$\omega^{WI} = \frac{(\Delta - \frac{\tilde{\theta}_w}{2})}{1+\frac{\theta_w^T\theta_w}{4}}\dot{\theta}_w \tag{35}$$

Since $C^{bW} = C_o C^{IW}$ and $\dot{C}^{IW} = C^{IW}\widetilde{\omega}^{WI}$, it then follows that

$$\dot{C}^{bW} = -\tilde{\omega}_o C_o C^{IW} + C_o C^{IW}\tilde{\omega}^{WI} \tag{36}$$

Then, we can find α, β, $\dot{\alpha}$ and $\dot{\beta}$ in terms of different variables. It should be noted that as the definition of Π implies, we still have local angles of attack varying along the missile even when the rigid-body angle of attack at the reference point is zero. That leads to the idea that in simple rectilinear flight, a missile can still experience aeroelastic deformation in various speed ranges. The above slender-body aerodynamics is thought to be relatively useful at the flight range below Mach 5 since above 5, more advanced and complicated aerodynamics caused by aerodynamic heating will be needed. Also, most full-scale tactical missiles operates at below Mach 4, so the current aerodynamics will be used in flight speed range between Mach 2 and Mach 5.

The normal force distribution acts as a distributed force along the body and at the same time, it works as a rigid-body force and a moment about the reference point. The distribution effect along the body and its implementation into the system equations are addressed in Appendix B due to length. The effects of normal force distribution on rigid body force and moment, and the implementation into the rigid-body system equations are dealt with in Appendix C for the same reason.

Results according to above formulation are in good agreement with existing experimental data. Fig. 3 represents the comparison between slender-body theory and experiments from [66] for steady flow when the angle of attack is 10° at Mach 2 for an ogive-cylinder configuration. The average normal force and pitching moment are in excellent agreement and the distributed force shows sufficiently good agreement for the purposes of our current research. Drag is very dependent on the configuration and flight condition. Body, wings and tails all make contributions to the drag, and the body drag is dominant especially in the supersonic flight regime. For the calculation of skin friction drag, a turbulent skin friction coefficient and laminar skin friction coefficient should be obtained. For most flight conditions laminar flow prevails over the extreme forward portion of the missile body, followed by completely turbulent flow over the remaining portion of the missile [67]. The difficulty lies in determining the transition point from laminar flow to turbulent flow. Since no theoretical methods are known to accurately determine the transition point, the point on the missile body where the Reynolds number reaches 10^6 is generally taken from experience and test

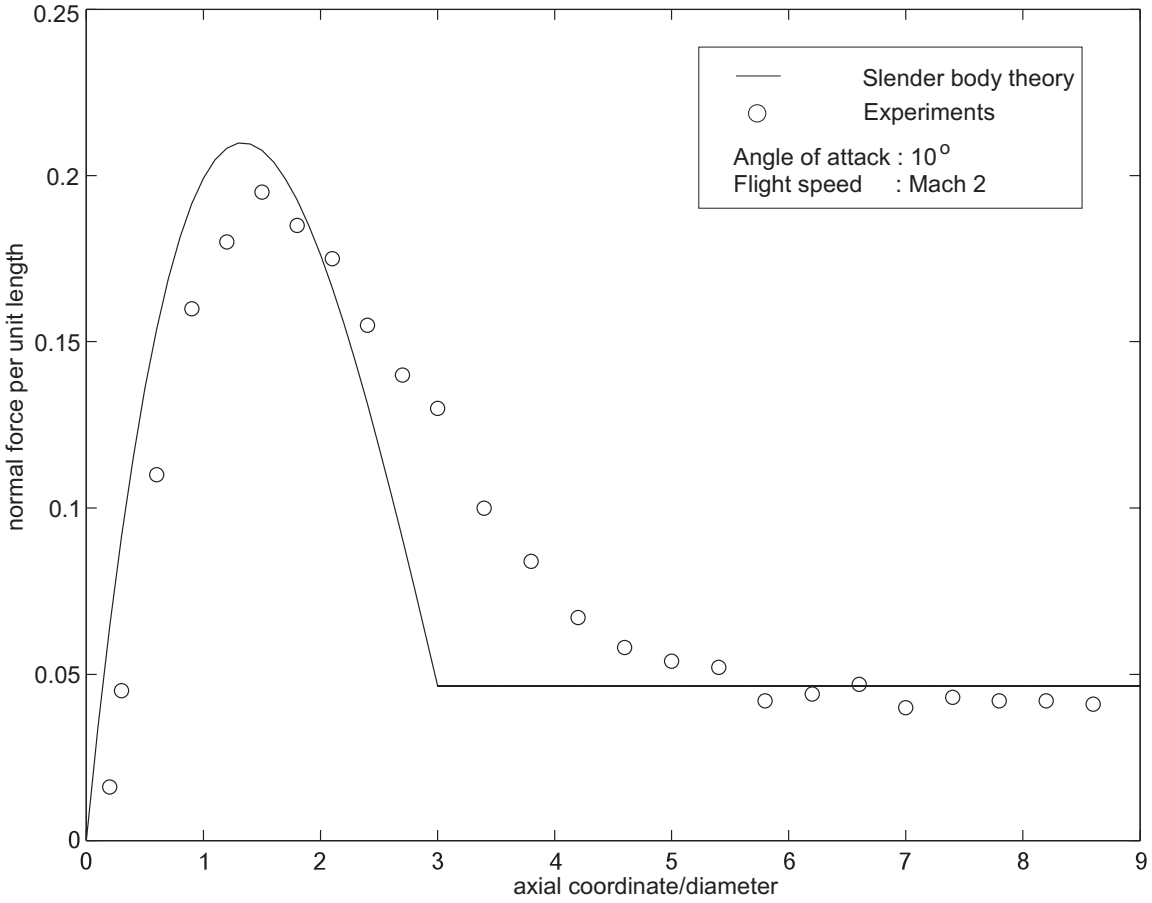

Fig. 3: Comparison of slender-body theory with experiments

data [59]. A reasonable assumption for a missile body with normal roughness it to take the nose tangency point at the end of the nose or forebody section as transition point [67]. Fig. 4 shows a typical drag distribution over missile body at supersonic flight. One engineering method for calculating skin-friction drag is to compute skin friction for an equivalent flat plate of the same surface area, length, and Reynolds number as the original body. The axial force is then corrected for body shape by the use of a three-dimensional shape factor. The method of [68] is used for mean skin friction coefficient of compressible flow on a two-dimensional flat plate, and a modified Blasius theory including compressibility effects, as discussed by [69], is used for laminar skin friction drag. To get the wave drag over the range of Mach number from $2 - 5$, the second-order shock expansion method (see [70]) or a modified Newton method is usually applied to the entire body. At the missile base, the pressure goes down below the freestream pressure due to the external flow. This base drag is highly dependent on Mach number and the presence of a boat tail or flare. For the purposes of the current research, methods based on approximate, closed-form solutions, or that at least require the least computational effort have been employed, such as the modified Newtonian method and tangent cone method. Also, in case of spin stabilized missiles, additional lift should be considered due to the effect of spin, which is called the Magnus effect; see [71]. All the available methods for missile aerodynamics are well documented in [61, 72].

The above discussed aerodynamics along with structural dynamics formulation will lead to a complete solution for aeroelastic stability problems for various

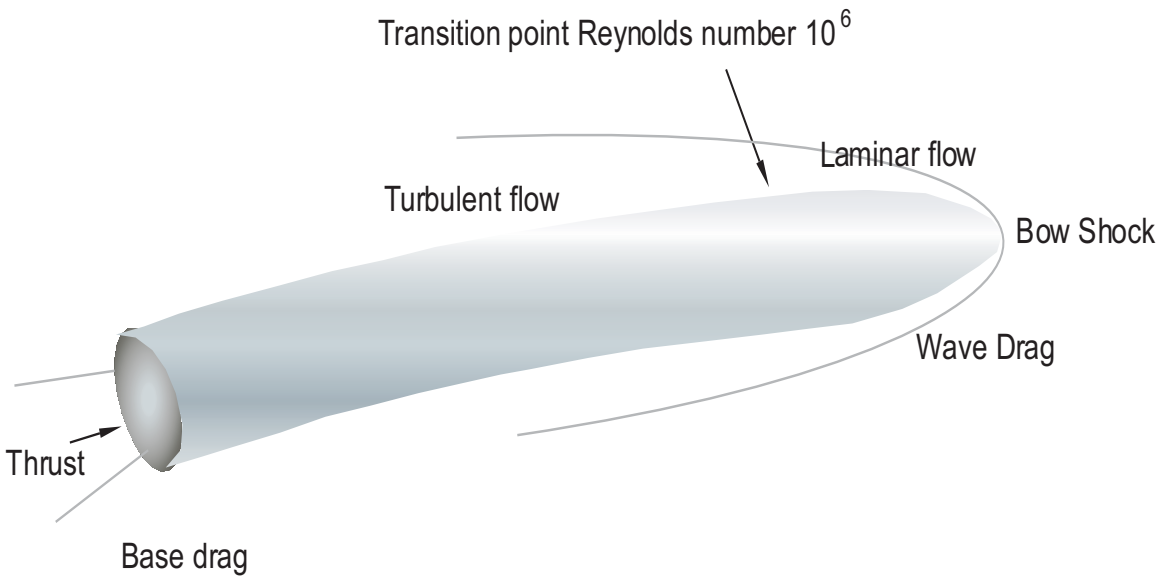

Fig. 4: Body drag distribution at supersonic flow

missiles and projectiles. Some additional variables such as acceleration, angular velocity and linear velocity at the final time of time interval, and direction cosine matrix will appear and they should be embedded properly in the system equations. This combined aeroelastic formulation will yield iterative solutions over time which affect both aerodynamic loads and structural loads.

4.3 Solution Methodology

Now space-time finite elements are used to obtain the time history of the missile motion, which is needed to investigate the nonlinear dynamics of the missile in flight. This kind of space-time finite element approach is useful in finding the amplitude of the limit cycle oscillations and checking the nonlinear system

response. To use this space-time finite element, the formulation should be converted into its weakest form in space as well as time. After integration by parts of the additional energy expression due to rigid-body motion, the unknowns are neither differentiated with respect time nor space from henceforth, so that constant shape functions may be used for them. Since the weak form is linear in the virtual quantities and they may be differentiated with respect to both space and time, and linear/bilinear shape functions are used for them, and element numerical quadrature is not needed. Thus,

$$
\begin{aligned}
&\overline{\delta q}_B = \overline{\delta q}_{i_s}(1-\xi)(1-\tau) + \overline{\delta q}_{i_f}(1-\xi)\tau \\
&\qquad + \overline{\delta q}_{i+1_s}\xi(1-\tau) + \overline{\delta q}_{i+1_f}\xi\tau && u = u_i \\
&\overline{\delta \psi}_B = \overline{\delta \psi}_{i_s}(1-\xi)(1-\tau) + \overline{\delta \psi}_{i_f}(1-\xi)\tau \\
&\qquad + \overline{\delta \psi}_{i+1_s}\xi(1-\tau) + \overline{\delta \psi}_{i+1_f}\xi\tau && \theta = \theta_i \\
&\overline{\delta F} = \overline{\delta F}_i(1-\xi) + \overline{\delta F}_{i+1}\xi && F = F_i \\
&\overline{\delta M} = \overline{\delta M}_i(1-\xi) + \overline{\delta M}_{i+1}\xi && M = M_i \\
&\overline{\delta P} = \overline{\delta P}_{i_s}(1-\tau) + \overline{\delta P}_{i_f}\tau && P = P_i \\
&\overline{\delta H} = \overline{\delta H}_{i_s}(1-\tau) + \overline{\delta H}_{i_f}\tau && H = H_i \\
&\delta q_o = \delta q_{o_s}(1-\tau) + \delta q_{o_f}\tau \\
&\delta \psi_o = \delta \psi_{o_s}(1-\tau) + \delta \psi_{o_f}\tau
\end{aligned}
$$

where subscripts s and f denote the variable values at the starting and final time of time interval. After some manipulations it can be shown that some of the resulting discretized equations are linear combinations of the others, leaving us free to discard the excess equations. For illustrative purposes, we consider only

the structural part for the time being. Then,

$$\overline{\delta q}_{if} \qquad \overline{P}_i = \frac{\hat{P}_{if} + \hat{P}_{is}}{2}$$

$$\overline{\delta \psi}_{if} \qquad \overline{H}_i = \frac{\hat{H}_{if} + \hat{H}_{is}}{2}$$

$$\overline{\delta P}_{if} \qquad \overline{u}_i = \frac{\hat{u}_{if} + \hat{u}_{is}}{2}$$

$$\overline{\delta H}_{if} \qquad \overline{\theta}_i = \frac{\hat{\theta}_{if} + \hat{\theta}_{is}}{2}$$

$$\overline{\delta q}_{n+1} \qquad \overline{F}_i = \frac{\hat{F}_i + \hat{F}_{i+1}}{2}$$

$$\overline{\delta \psi}_{n+1} \qquad \overline{M}_i = \frac{\hat{M}_i + \hat{M}_{i+1}}{2}$$

$$\overline{\delta F}_{n+1} \qquad \overline{u}_i = \frac{\hat{u}_i + \hat{u}_{i+1}}{2}$$

$$\overline{\delta M}_{n+1} \qquad \overline{\theta}_i = \frac{\hat{\theta}_i + \hat{\theta}_{i+1}}{2}$$

$$\delta q_{of} \qquad \overline{P}_o = \frac{\hat{P}_{of} + \hat{P}_{os}}{2}$$

$$\delta \psi_{of} \qquad \overline{H}_o = \frac{\hat{H}_{of} + \hat{H}_{os}}{2}$$

By virtue of these relations, the number of unknowns corresponding to each virtual quantity is reduced. Then, the total number of equations related to elastic variables; $\overline{\delta q}_{is}$, $\overline{\delta \psi}_{is}$, $\overline{\delta P}_{is}$, $\overline{\delta H}_{is}$, $\overline{\delta F}_i$, $\overline{\delta M}_i$ (i=1 to n), is $18n$. The total number of equations defining rigid-body motion related to $\delta q_{os}(3)$, $\delta \psi_{os}(3)$, $\delta v_o(3)$, $\delta \omega_o(3)$, is 12 if we do not consider direction cosine and acceleration variables. Unknown variables are $\hat{F}_i$, $\hat{M}_i$, $\hat{P}_{if}$, $\hat{H}_{if}$, $\hat{u}_{if}$, $\hat{\theta}_{if}$, $\hat{P}_{of}$, $\hat{H}_{of}$, $\hat{v}_o$, $\hat{\omega}_o$ after specifying boundary conditions ($\hat{F}_{n+1}$, $\hat{M}_{n+1}$ and $\hat{u}_1$, $\hat{\theta}_1$) and initial conditions ($\hat{P}_{is}$, $\hat{H}_{is}$, $\hat{u}_{is}$, $\hat{\theta}_{is}$, $\hat{P}_{os}$, $\hat{H}_{os}$) for each element, therefore in total $18n$ +12. The above discussion shows that the total number of equations and the total number of unknowns are equal.

With these system equations and unknown variables, if we just consider structural dynamics, the mixed variational formulation takes the form

$$F(X_s, X_f, X) = 0 \tag{37}$$

where X is a column matrix of all structural variables and X_s and X_f are its initial and final values. This nonlinear algebraic equation can be solved by Newton-Raphson. The Jacobian matrix of the above set of nonlinear equations can be obtained analytically or numerically and is found to be extremely sparse due to the formulation's weakest form. This helps to obtain the high computational efficiency. So, if the initial conditions and boundary conditions are specified, the final values after one time step can be found very efficiently using the damped Newton-Raphson method, and time history is obtained by doing time marching iteration. The structural part of the above formulation has been well validated against the stability subject to thrust. Fig. 5 shows more specific time-marching scheme.

The computer program was developed to run the nonlinear aeroelastic stability problems in various situations. The running results give time history for each variable. To solve the system of nonlinear algebraic equations, this program uses multi-variable damped Newton-Raphson method. The system equations and Jacobian matrix are calculated at each iteration. After setting up linear system equations from nonlinear algebraic system equations, linear system equations are solved with help of the Harwell Math Library's subroutines.

This program requires input of model file and initial condition set-up files. Once those data files and initial conditions are taken, the code runs continuously

over the specified time. Results at each iteration are iteratively taken as initial guesses and initial conditions for time-marching. This nonlinear aeroelastic code is used for either only thrust-induced stability or full analysis for a complete missile.

Apart from the above discussion, several issues on computational stability and efficiency should be addressed. First, the kinematic quantities for initial conditions should satisfy certain kinematical relations since they are not independent. So if one variable is perturbed, other variables are affected; that is, all the kinematic quantities which are related to it should have modified values. This is an important aspect of the formulation, since it predominantly affects the sensitivity and convergence of the solution for the time-marching scheme. Second, depending on the type of problems proposed, some variables can be added or removed for computational efficiency. For example, for rectilinear flight, direction cosine variables would not be needed. Missile aerodynamics discussed will need additional variables and equations such as acceleration and direction cosines and related equations.

4.4 Nonlinear Stability Analysis without Aerodynamics

Based on the methodology set forth here, a computer code for investigation of the nonlinear dynamics of a missile has been developed. The various stability problems due to thrust which appear in the literature can be examined in terms of their time history. First, for validation purpose of the current work, the case

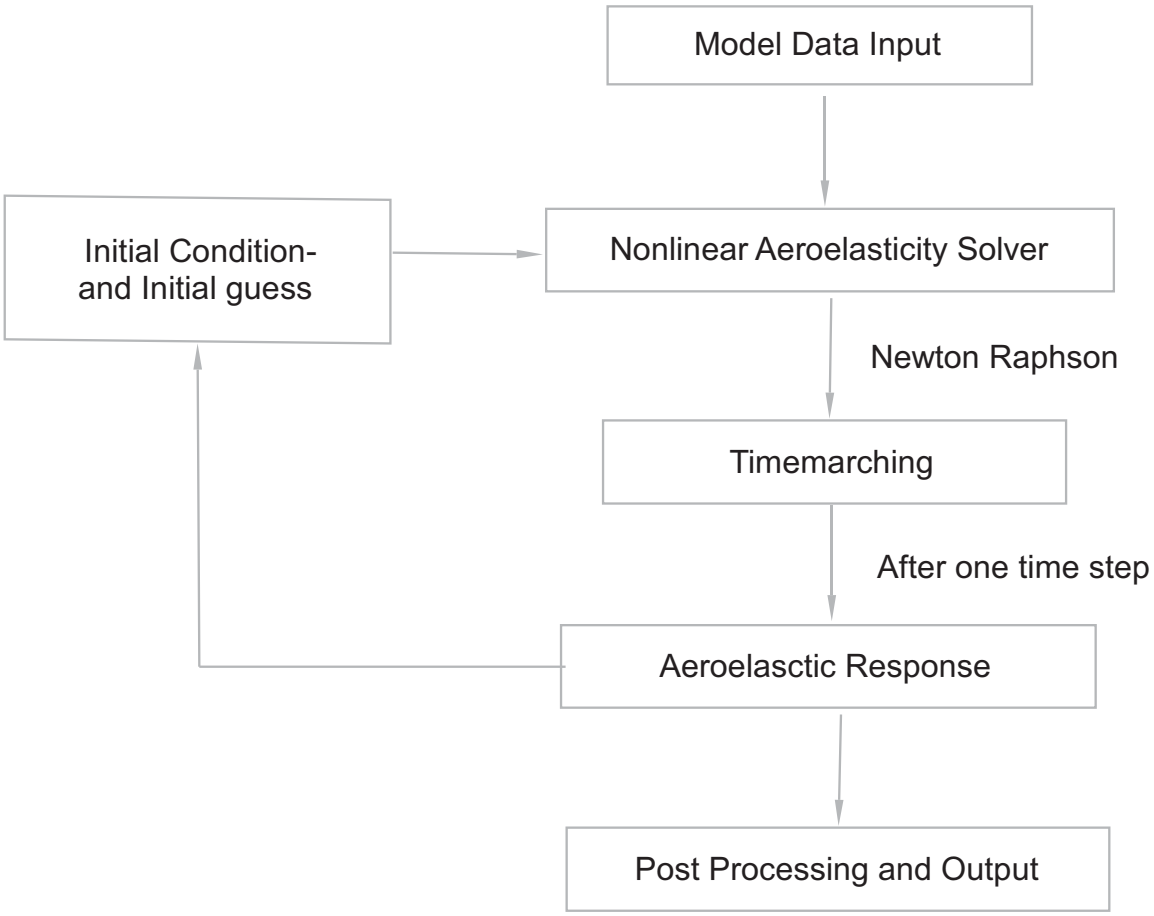

Fig. 5: Time-marching scheme

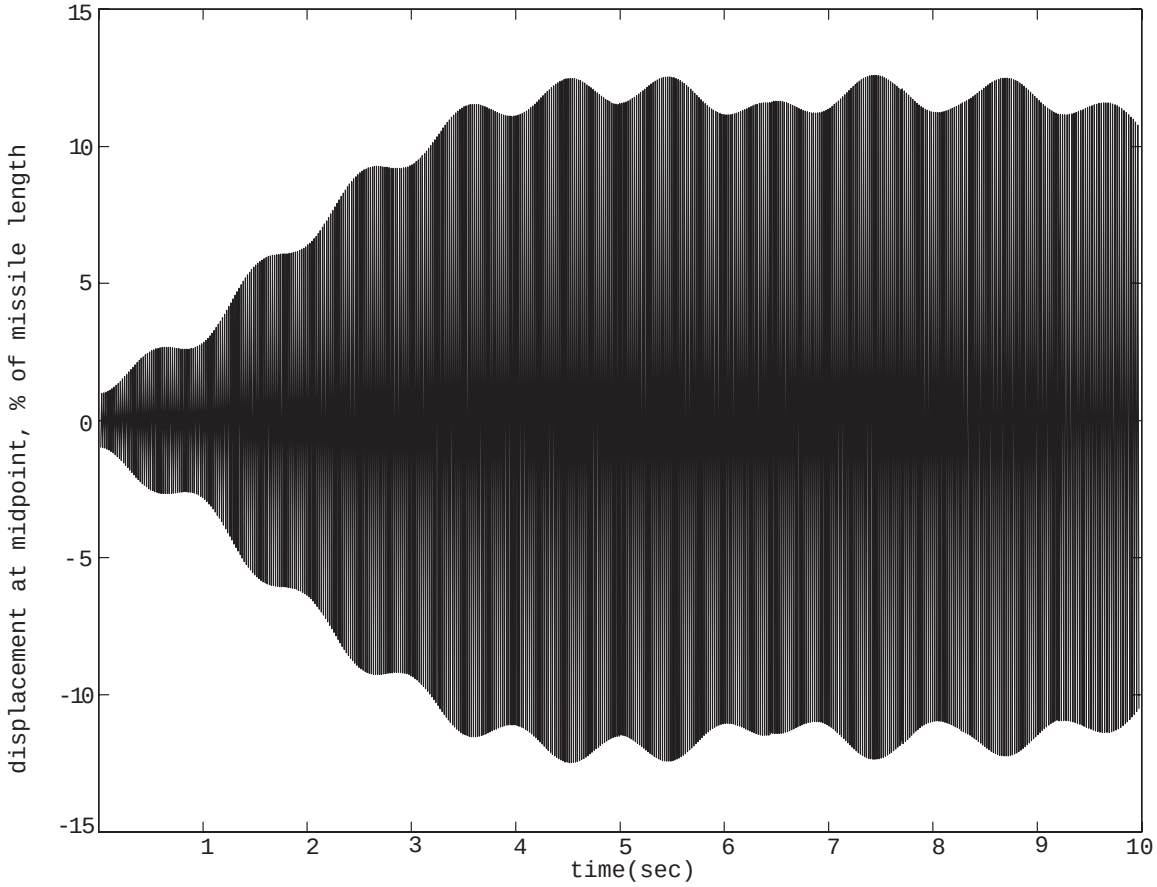

Fig. 6: Time history above critical thrust

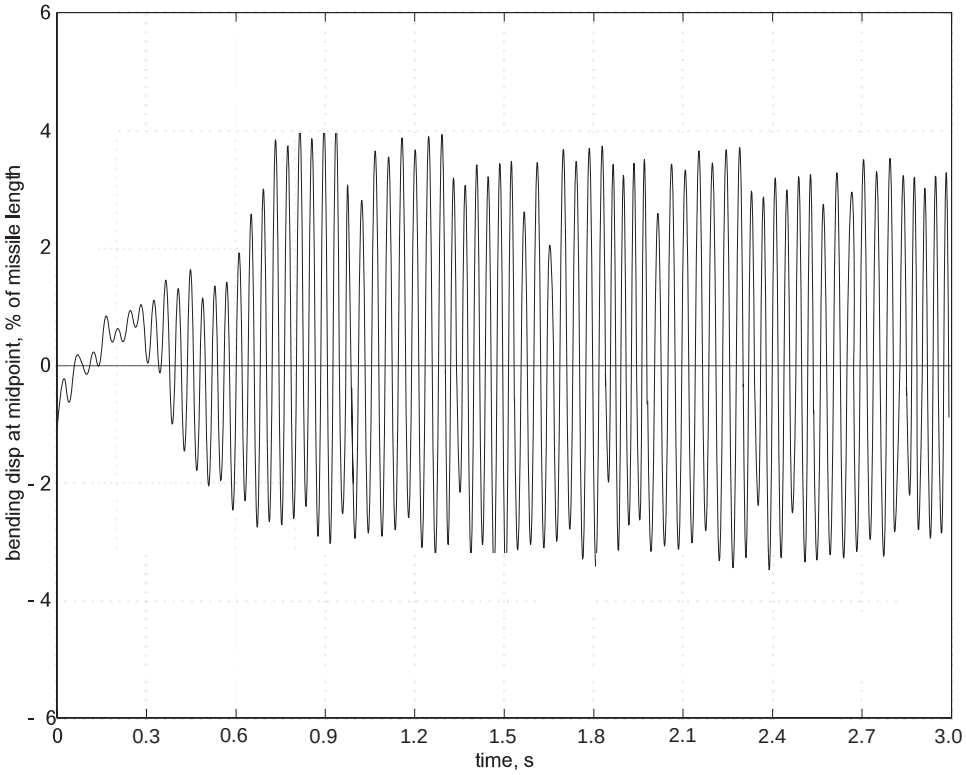

Fig. 7: Time history below critical thrust

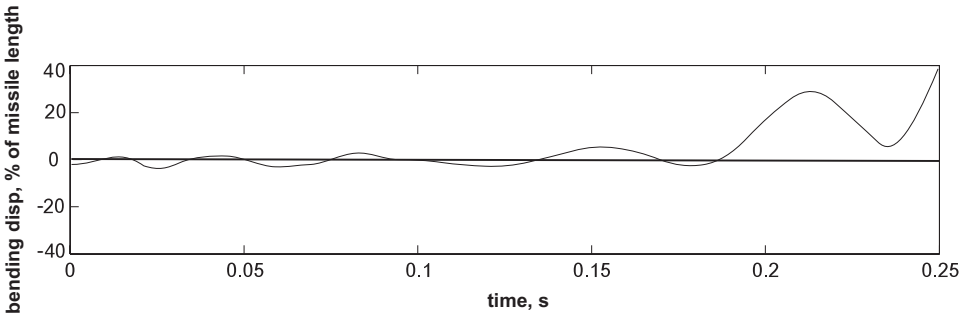

Fig. 8: Time history well above critical thrust

without directional control considered by [1] is addressed. Since it is known that the mass distribution also contributes to the critical load for thrust, constant mass will be considered for a comparison purpose. Also, zero shear deformation will be assumed for simplicity. When a small perturbation of the transverse deflection is imposed at the initial time and the thrust level is below Beal's critical value ($\frac{Thrust*length^2}{Bending\ stiffness}$=109.9), the deflection indeed dies out in time. However, as expected, when the thrust level is a little larger than the critical value, the deflections grow until they reach an oscillatory motion with bounded amplitude, suggesting a limit cycle. For comparison reasons, the same initial deflections were applied to the following each case. Results show that limit cycles can develop from disturbances with thrust values that are either just below the critical value suggested by [1] or just above it. Fig. 6 shows a bounded amplitude over time when the the thrust level is 1.02 times the Beal's critical value. Fig. 7 shows a limit cycle when thrust level is 0.95 times the Beal's critical value. However, the motion is divergent when thrust level is 1.4 times the critical value as shown in Fig. 8. It should be noted that the amplitude of the response shown in Fig. 8 is much bigger than that of the response in Fig. 7, in fact, the response goes beyond 40% of the missile length within very small time (0.25 second). This observation serves to partially validate the current approach.

4.5 Ballistic Flight

To see if there are any aeroelastic effects on the stability as a function of thrust or on accelerated flight, Fig. 9 is used as a baseline missile configuration; see

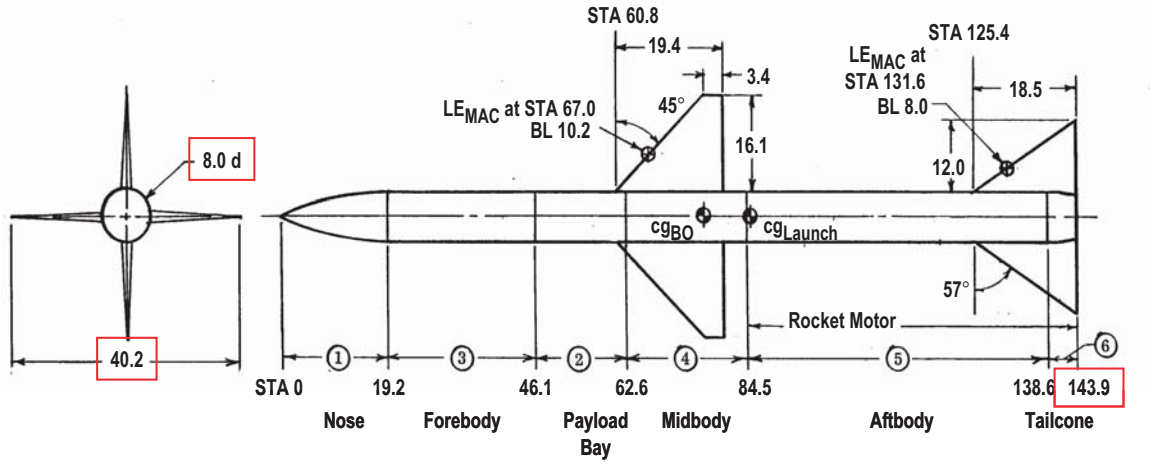

Fig. 9: Baseline missile configuration

Table 1: Test case data, ballistic flight

Bending Stiffness:	uniform 2×10^6N-m^2
Altitude:	20 km
Density:	0.0889 kg/m^3
Temperature:	216.7K

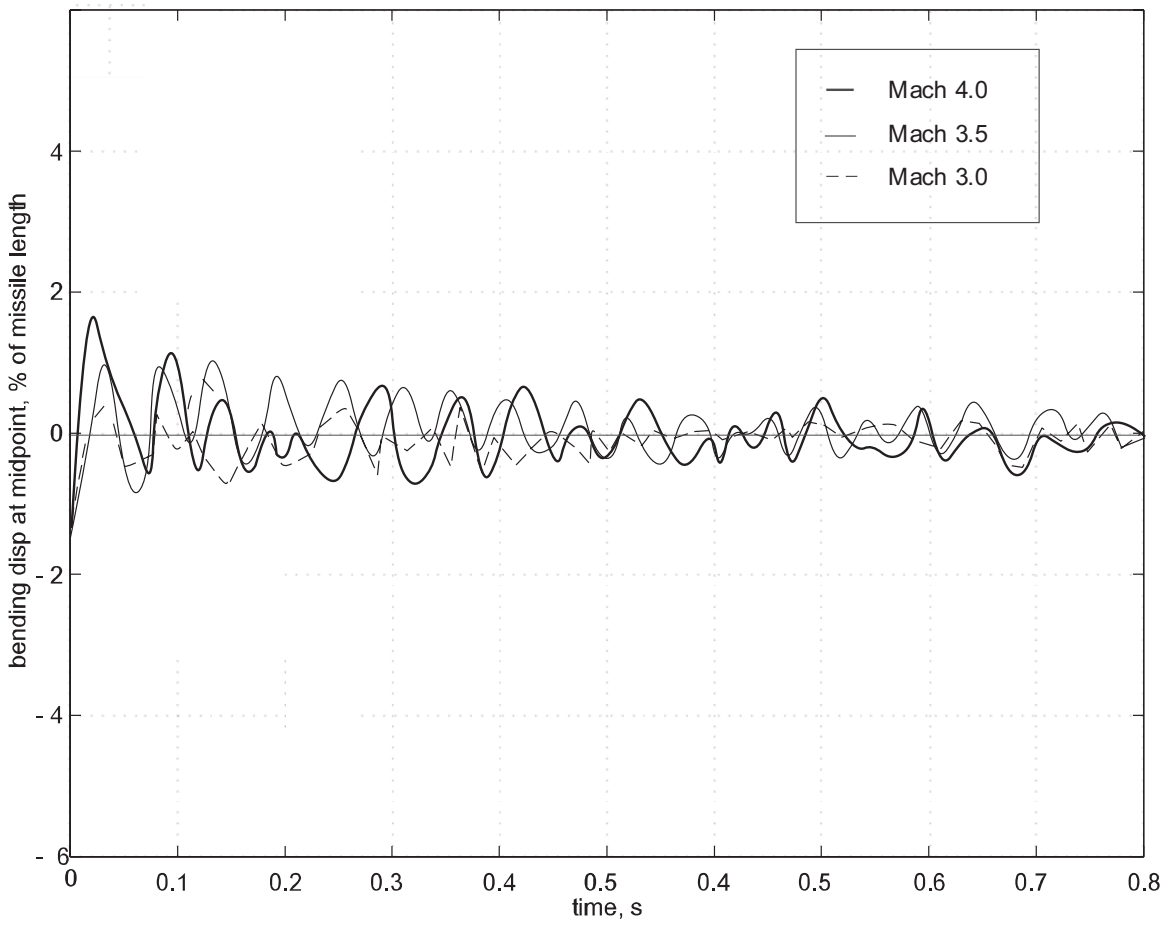

Fig. 10: Stability for ballistic flight case

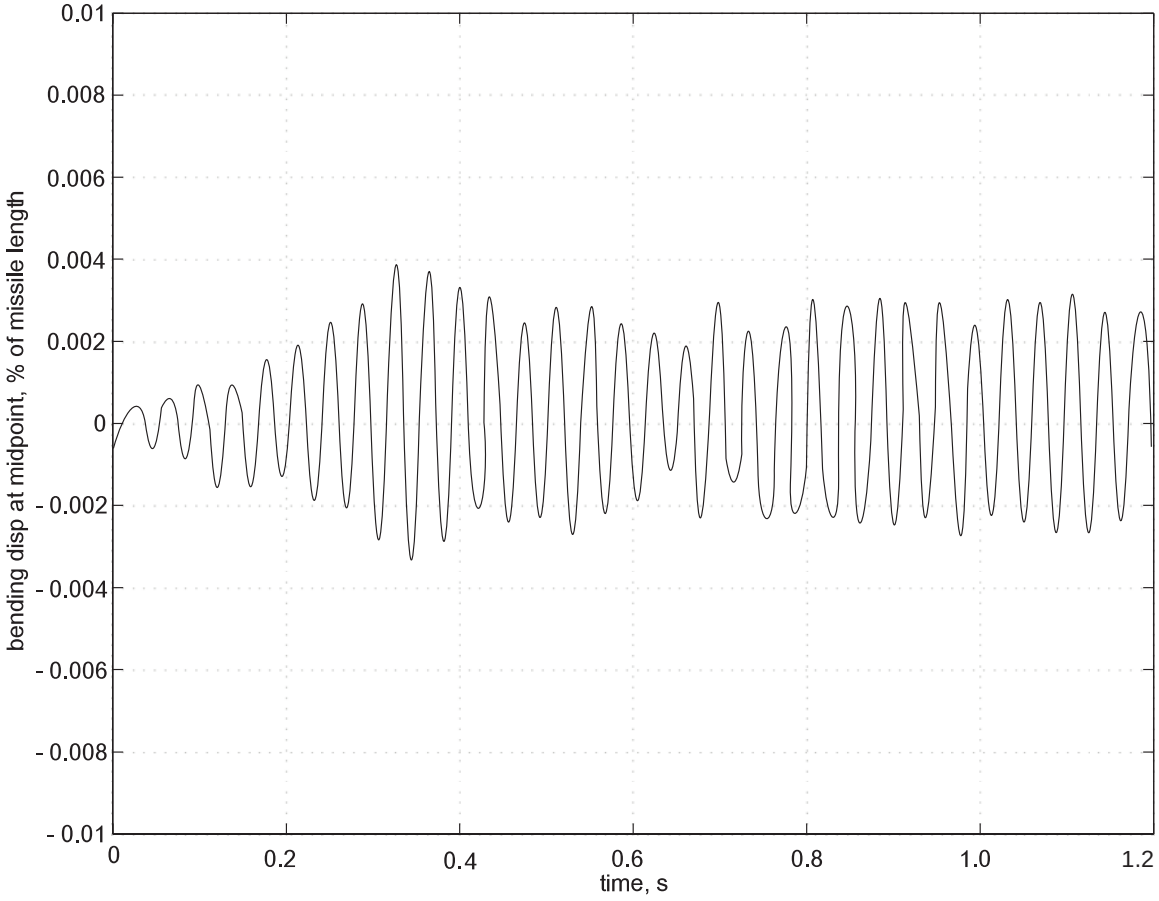

Fig. 11: Effect of reduced bending stiffness on stability in ballistic flight

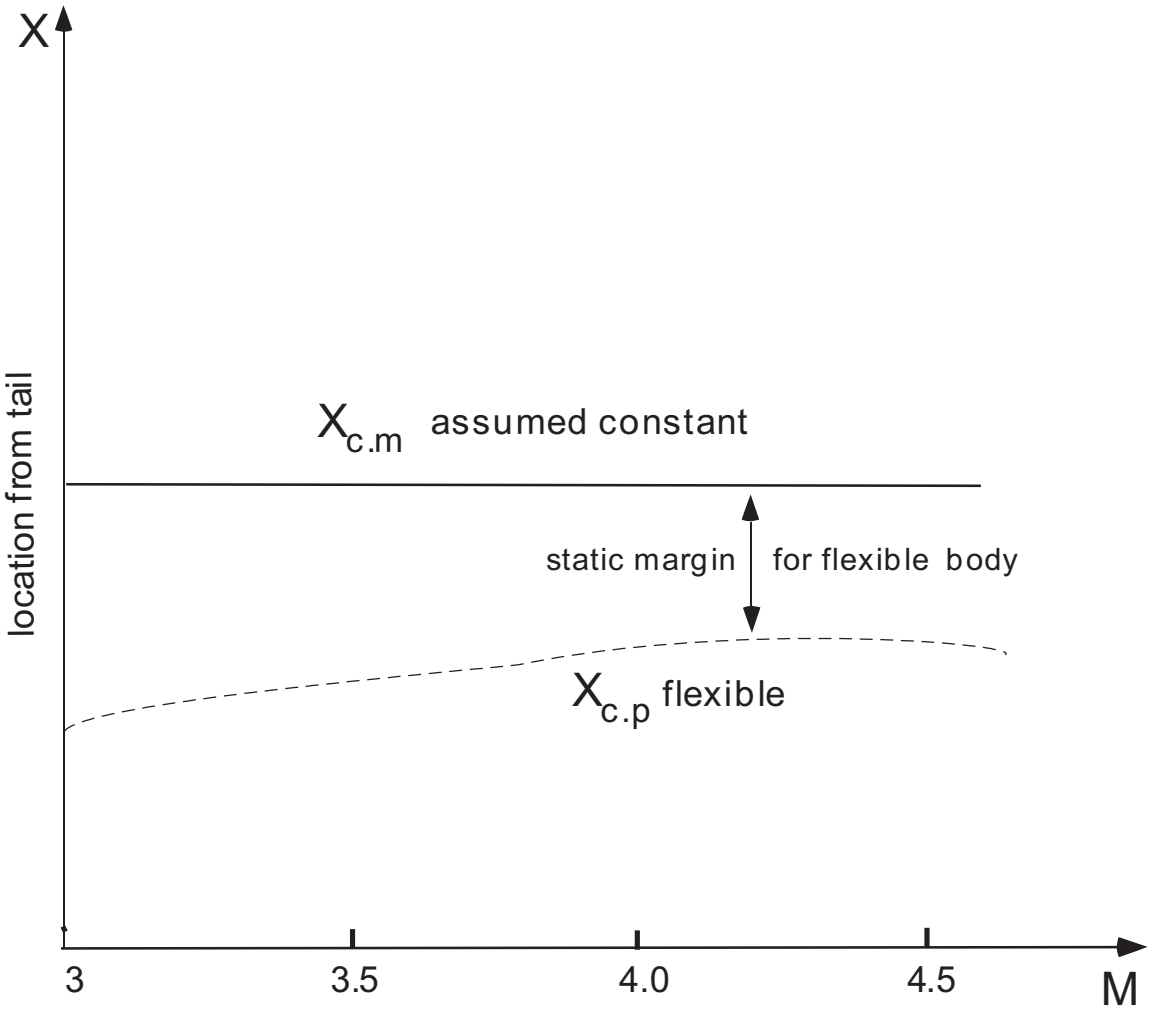

Fig. 12: Static stability showing static margin

[73]. Both movable wings and fixed tail fins with a cruciform pattern have two sets of wedge-shaped panels. Around the nose, the large missile body drag is applied. The fins and tail are both under the influence of wave drag and skin friction drag. At the nozzle base, base drag and thrust are both applied. The total drag force is distributed along the body. Here it should be noted that missile fins are not a consideration for stability because we are interested in only missile body bending modes. The loads on the fins are applied as concentrated forces. In reality, missile fin flutter is more common phenomena since fins are more flexible compared to the missile body. But the purpose of this research is to identify how bending of the missile body affects aeroelastic stability. Therefore, this assumption will be maintained under the current research. The basic idea about how the aeroelastic phenomena occur is that missile bending will change the local angle of attack on the body and the changed local of attack will in turn give different aerodynamic loads on the missile, which will further deform the missile. This iterative process of yielding new aerodynamic loads and deforming the missile will result in stable or unstable flight depending on the various flight conditions and missile characteristics.

When the thrust force is balanced with the total drag, the missile maintains equilibrium by flying at constant speed. But depending on whether the thrust force magnitude is bigger or smaller than the total drag, the missile either accelerates or decelerates. First the aeroelastic stability of missile flying at high supersonic velocity will be addressed. Once velocity is specified, the missile drag

is determined from unsteady aerodynamics for missiles. The initial flight condition satisfying kinematic relations and initial deflection for bending are given to run this case. Fig. 10 shows the bending response in rectilinear flight for the test case from Table 1. The case represents deceleration from steady-state flight with each Mach number as an initial speed. The responses showed that there was no aeroelastic instability for the uniform bending stiffness in this test case. With a very small time interval, less than one second was good enough to identify the decay. The velocity increase noticeably affects the amplitudes of the response after small lateral disturbances are given. The flexural stiffnesses are relatively large, but the distributed drag forces appear to play the role of reducing the effective stiffness. To see the effect of bending stiffness on aeroelastic stability in ballistic flight, the size of bending stiffness was reduced to about 1/100 of the original value. Fig. 11 shows limit cycle when the initial speed is Mach 4.0 with the reduced bending stiffness. One can see the conspicuous effect of bending stiffness on the aeroelastic stability at ballistic flight.

Under the current formulation, the total mass of the missile does not change. Thus, the center of mass location along the missile axis is assumed to be constant, and the center of pressure of missile can be calculated from running the code. From Fig. 12 one can see that this flexible missile body model is statically stable. In reality the missile center of mass moves closer to missile nose as the fuel is consumed. Therefore, the body will have a little larger static margin.

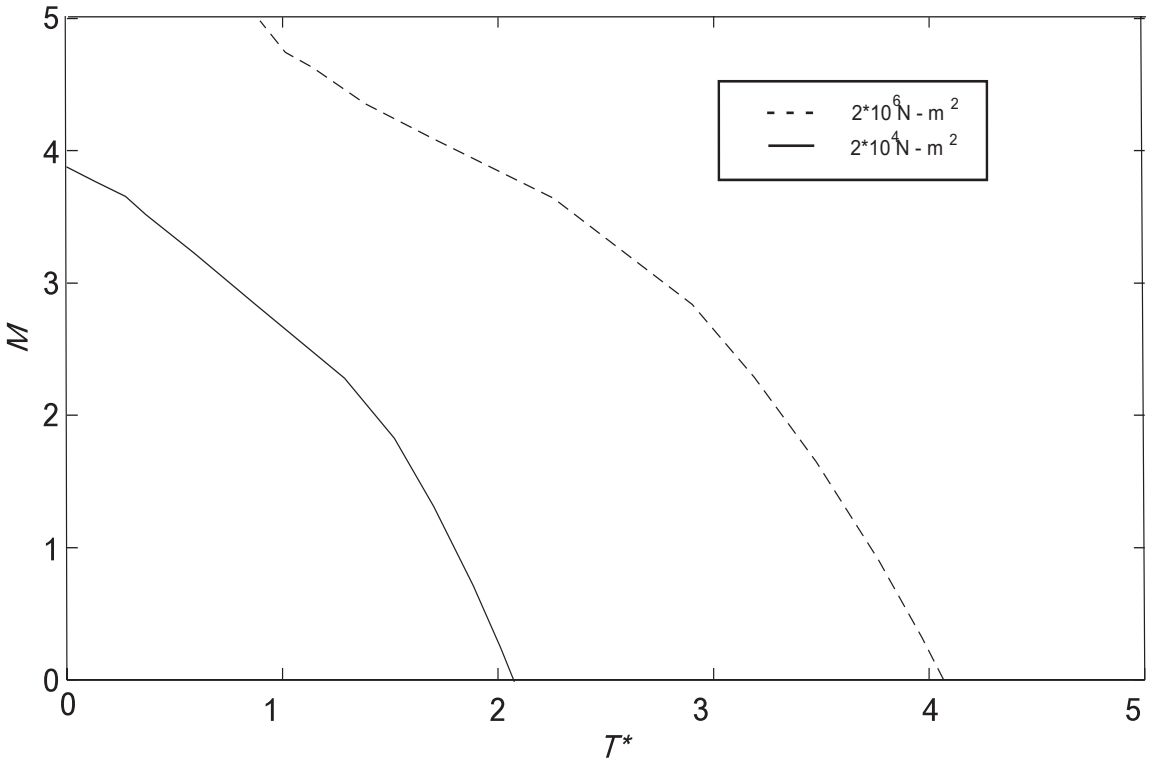

Fig. 13: Variation of flexibility

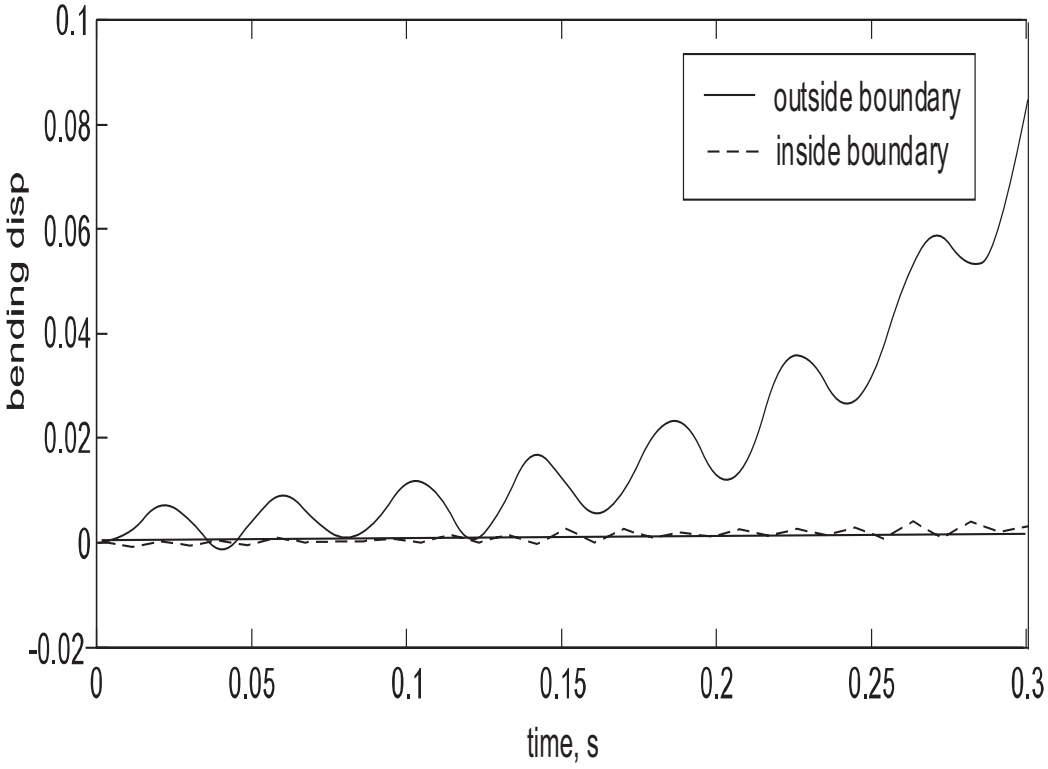

Fig. 14: Responses well above and below flutter point

4.6 Aeroelastic Effects of Thrust

As shown in previous sections, thrust and aerodynamic forces themselves have a destabilizing effect on the missile stability. Aeroelastic interactions between structural load, aerodynamic load, and inertial load are a continuous iterative process between each load. That is, the missile bending brought on by aerodynamic normal forces will change the local angles of attack along the missile body. Altered angles of attack will, in turn, change the aerodynamic forces on the missile body. That will yield additional inertial loading over the missile body. And these inertial loading further deforms the missile body. During this iteration, the missile will reach an equilibrium state where all the forces are balanced.

Besides all this, thrust will also influence the results. It is natural to ask how thrust interacts with aerodynamics. To answer that question, in this section several parametric studies will be presented. First, to see the aeroelastic effects of thrust, the flutter boundary is found for several different bending stiffnesses. To locate flutter points, more than 2 seconds of time-marching was needed. The reason for this is because, in the case of a limit cycle, the code had to be run iteratively to find a decay. Once the decay is found by reducing the flight speed from high values at a thrust level with a given bending stiffness, the flutter point is determined. Such a process is repeated with a different thrust level for a complete curve.

Fig. 13 shows the stability boundary for two different bending stiffnesses at the same altitude. Here $T^* = \log_{10}(T/mg)$. According to these results, it seems that thrust is a little bit more influential than aerodynamic force near thrust

equal to zero, *i.e.*, ballistic flight. A small addition of thrust will significantly reduce the flutter speed. Also it can be seen that when thrust is a dominant factor on stability, aerodynamic forces have less effect than thrust, that is, addition of aerodynamics will not greatly reduce the flutter thrust level. It appears that the curve close to the thrust abscissa has acceleration dominant stability and the curve close to ballistic flight has deceleration dominant. From the limitation of the current slender-body aerodynamics, some caution should be taken: It is meaningless to run a case at a higher flight speed than Mach 5. Considering the realistic value for bending stiffnesses, at this altitude, the dashed line results are more likely to occur. When obtaining each flutter point, limit cycles appeared either a little below or above the flutter speed. That means there is a certain mechanism, which is inherently nonlinear, to prevent immediate structural failure. Fig. 14 shows bending deflection responses by changing thrust level at Mach 3 for the bending stiffness 2×10^4N-m^2. The solid line was obtained about thrust level outside the flutter curve where T^* is 0.897 and dashed line about thrust level inside the flutter curve where T^* is 0.655. Well above flutter speed and thrust level, the response becomes unbounded within a very small time.

From the above discussion, it was seen that missile thrust, a follower force, affected the system's aeroelastic instability. This provides compelling reasons to explore another kind of follower force, say from an engine attached to a flexible wing. A big difference will be in the aerodynamics, but the same mixed variational formulation can be used for both systems. This mixed variational finite-element analysis tool allows two different approaches. The first approach is

a time-marching scheme and it is used for missile analysis. This time-marching scheme could be obtained by transferring the formulation to the weakest form in space and time, thereby making possible the use of simple finite elements in space and leading to nonlinear algebraic equations. Another is an eigenvalue analysis, which is obtained by transferring the mixed variational formulation to the weakest form in space. This leads to use of finite elements in space and a set of ordinary nonlinear differential equations in time. Next, the steady-state solution is obtained by using finite elements in space, and one can get linearized equations from the steady state for stability analysis. The second approach will be used to analyze the aeroelastic stability of a wing subjected to engine thrust. Note that in the aircraft, it is easier to define the trim state than for missiles.

CHAPTER V

EFFECT OF FOLLOWER FORCE ON WING FLUTTER

Now, another follower force that can be observed in aerospace structures will be discussed. The effect of thrust on the flutter of a high-aspect-ratio wing is investigated. The wing is represented by a beam using a nonlinear, mixed finite element method. Aerodynamic forces are calculated using a finite-state, two-dimensional unsteady aerodynamic model. The effect of thrust is modeled as a follower force of prescribed magnitude. Without the thrust force, the wing is shown to become unstable for freestream airspeeds greater than the flutter speed. On the other hand, in the absence of aerodynamic forces, the wing becomes unstable for values of the thrust in excess of a critical magnitude of the force. When both effects are present, the airspeed at which the instability occurs depends on the thrust magnitude. For validation and comparison, an analytical solution for the *in vacuo* case (accounting only for the effect of thrust) was developed and shown to closely match results from the numerical method. Parametric studies show that the predicted stability boundaries are very sensitive to the ratio of bending stiffness to torsional stiffness. Indeed, the effect of thrust can be either stabilizing or destabilizing, depending on the value of this parameter. An assessment whether or not the magnitude of thrust needed to influence the flutter speed is

practical is made for one configuration.

It is the objective of the present study to determine whether or not the thrust of wing-mounted engines might have any effect on the aeroelastic flutter of wings. In order to carry out this objective, the analytical solution for instability due to thrust alone is first developed without consideration of aerodynamic effects. This solution is then used for validating the finite element methodology for determining the influence of thrust on the aeroelastic stability. A mixed finite element method is then used to compute the instability boundary of the system under the influence of both effects. A parametric study focusing on the influence of the ratio of bending to torsional stiffness is also conducted. Finally, the thrust required to maintain the trim condition of a complete airplane model is estimated at various speeds and is used to determine the range of thrust values that can be considered as realistic. Analytical analysis on thrust-induced flutter is addressed more extensively in [74], and aeroelastic analysis of an engine thrust is quoted at length from [75].

5.1 Analysis of Thrust-Induced Flutter

Consider a cantilevered beam with elastic axis along the x_1 direction, and with cross-sectional coordinates x_2 and x_3 as shown in Fig. 15. The beam has torsional stiffness GJ and bending stiffnesses EI_2 and EI_3 with $EI_3 >> EI_2$. Denote the displacements as u_i with $i = 1$, 2, and 3 along x_i directions, and denote the section rotation due to torsion as θ_1. For the purpose of analysis, we introduce two sets of dextral triads of unit vectors, one fixed in an inertial frame of reference,

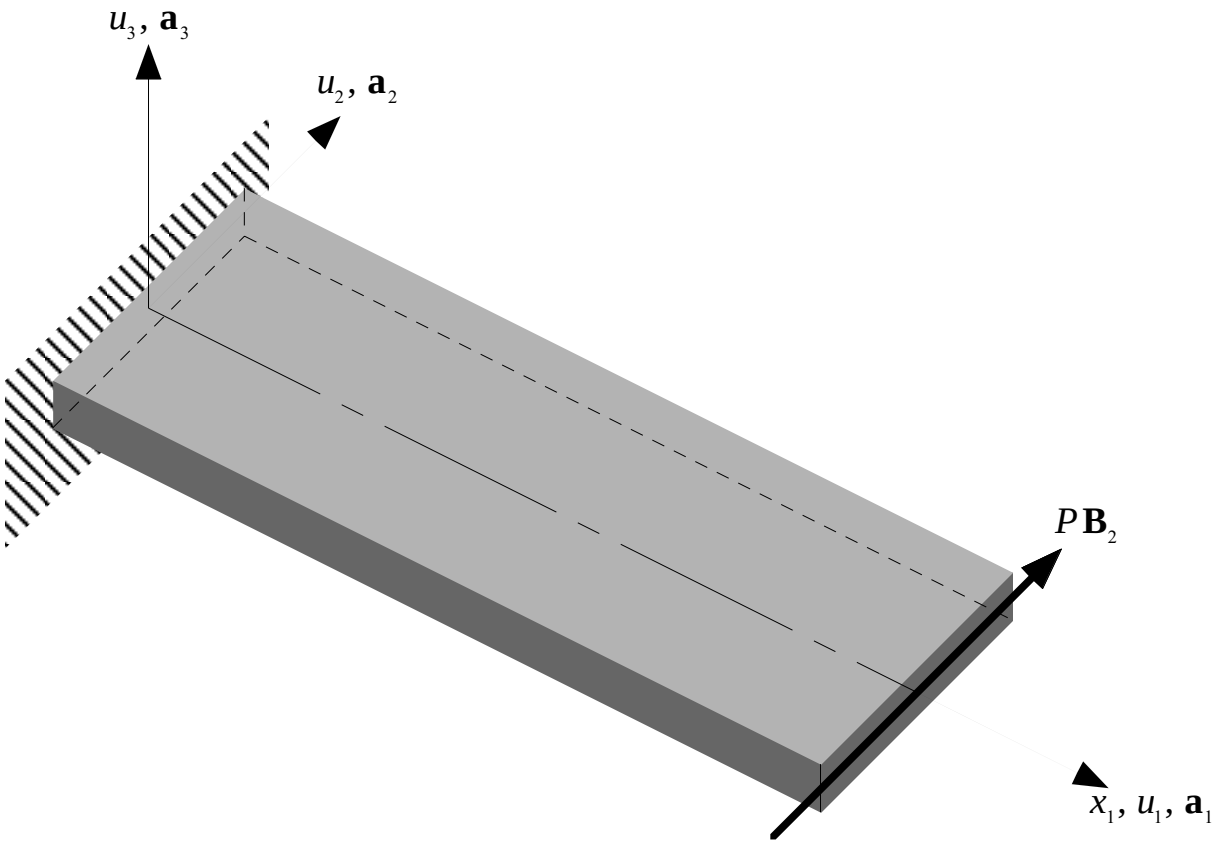

Fig. 15: Schematic of wing showing coordinate systems and follower force

$\mathbf{a}_i$ with $i = 1$, 2, and 3, along x_i, and the other fixed in the cross-sectional frame of the deformed beam, $\mathbf{B}_i$ with $i = 1$, 2, and 3. A load P is applied at the tip of the beam and is directed along unit vector $\mathbf{B}_2(\ell, t)$ where $\mathbf{B}_2(\ell, t) = -u_2'(\ell, t)\mathbf{a}_1 + \mathbf{a}_2 + \theta_1(\ell, t)\mathbf{a}_3$ and where $(\,)'$ is the partial derivative with respect to x_1. Thus, the virtual work done by this force through a virtual displacement is

$$\begin{aligned} \overline{\delta W} &= P\mathbf{B}_2(\ell, t) \cdot [\delta u_1(\ell, t)\mathbf{a}_1 + \delta u_2(\ell, t)\mathbf{a}_2 + \delta u_3(\ell, t)\mathbf{a}_3] \\ &= P\left(-u_2'\delta u_1 + \delta u_2 + \theta_1 \delta u_3\right)\Big|_0^\ell \end{aligned} \tag{38}$$

In keeping with the nonconservative nature of the follower force, there is no potential energy expression, the variation of which, will yield this expression for the virtual work. We will subsequently ignore the longitudinal displacement u_1.

For a beam subject to a bending moment $\overline{M}_3$ that is constant in time but varying in x_1, and in which deflections due to that moment are ignored (since $EI_3 >> EI_2$), the strain energy can be written as

$$U = \int_0^\ell \left[\frac{GJ}{2}{\theta_1'}^2 + \frac{EI_2}{2}u_3''^2 + \overline{M}_3\left(u_2'' + \theta_1 u_3''\right)\right] dx_1 \tag{39}$$

For static deformation of the beam, one may consider only the first-order terms in $\delta U - \overline{\delta W}$, such that

$$\int_0^\ell \left(\overline{M}_3 \delta u_2'' - P\delta u_2'\right) dx_1 = 0 \tag{40}$$

Thus,

$$\overline{M}_3 = P(\ell - x_1) \tag{41}$$

as expected. To obtain a weak form that governs static behavior, one may set

the second-order terms in $\delta U - \overline{\delta W}$ equal to zero, so that

$$\begin{aligned}\delta U - \overline{\delta W} = \int_0^\ell \big[& EI_2 u_3'' \delta u_3'' + GJ\theta_1' \delta\theta_1' \\ & + P(\ell - x_1)(\theta_1 \delta u_3'' + u_3'' \delta\theta_1)\big] dx_1 \\ & - P\theta_1 \delta u_3 \Big|_0^\ell = 0\end{aligned} \tag{42}$$

Integrating by parts, one can eliminate the trailing term so that

$$\begin{aligned}\delta U - \overline{\delta W} = \int_0^\ell \big\{ & EI_2 u_3'' \delta u_3'' + GJ\theta_1' \delta\theta_1' \\ & + P\left[(\ell - x_1)\theta_1\right]'' \delta u_3 \\ & + P(\ell - x_1) u_3'' \delta\theta_1 \big\} dx_1 = 0\end{aligned} \tag{43}$$

It can be shown that there is no value of P that will result in buckling. Thus, one must add the kinetic energy and consider the stability of small vibrations about the static equilibrium state.

The kinetic energy of the vibrating beam with mass per unit length of m, radius of gyration of $\overline{\sigma}$ and mass offset $\overline{e}$, is simply

$$K = \frac{1}{2} \int_0^\ell \left(m\dot{u}_2^2 + m\dot{u}_3^2 + m\overline{\sigma}^2 \dot{\theta}_1^2 + 2m\overline{e}\dot{\theta}_1 \dot{u}_3 \right) dx_1 \tag{44}$$

where $\dot{(\,)}$ is the partial derivative with respect to time.

We now undertake a straightforward application of Hamilton's principle

$$\int_{t_1}^{t_2} \left(\delta U - \overline{\delta W} - \delta K \right) dt = 0 \tag{45}$$

where t_1 and t_2 are fixed times. Integrating by parts in time, setting δu_3 and $\delta\theta_1$ equal to zero at the ends of the time interval, removing the time integration, introducing a set of nondimensional variables, and assuming that the motion

variables are proportional to $e^{\overline{s}t}$, one obtains a weak form that governs the flutter of a beam subjected to a transverse follower force given by

$$\begin{aligned}\int_0^1 \Big\{ & \sqrt{\lambda} w'' \delta w'' + \sqrt{\frac{1}{\lambda}} \theta' \delta\theta' \\ & + s^2 \left[w\delta w + e\left(w\ \delta\theta + \theta\ \delta w\right) + \sigma^2 \theta\ \delta\theta \right] \\ & + p(1-x) w'' \delta\theta + p[(1-x)\theta]'' \delta w \Big\} dx = 0\end{aligned} \tag{46}$$

where

$$\begin{aligned} (\ )' &= \frac{d(\ )}{dx} & x_1 &= x\ell \\ u_3 &= \ell w e^{s\psi} & \theta_1 &= \theta e^{s\psi} \\ \psi &= \sqrt{\frac{\sqrt{GJ\,EI_2}}{m\ell^4}}\, t & \lambda &= \frac{EI_2}{GJ} \\ p &= \frac{P\ell^2}{\sqrt{GJ\,EI_2}} & s^2 &= \frac{m\ell^4 \overline{s}^2}{\sqrt{GJ\,EI_2}} \\ \sigma &= \frac{\overline{\sigma}}{\ell} & e &= \frac{\overline{e}}{\ell} \end{aligned} \tag{47}$$

This weak form can be solved approximately by assuming a set of cantilever beam free-vibration modes for bending and torsion. Specifying values for λ, e, and σ, one can solve for the real and imaginary parts of s as functions of p. Depending on the values chosen for λ, e, and σ, flutter will occur either along with the coalescence of two bending modes or with the coalescence of a bending mode and a torsional mode.

5.2 Incorporation of Aeroelastic Effects

The analysis methodology explained in the earlier section solves the problem of instabilities induced by a transverse follower force. One of the goals of the present

work is to investigate the instabilities due to the action of both the thrust and the unsteady aerodynamic forces. Such an analysis is quite complex and needs to be done using a numerical solution methodology. The present work uses mixed finite element modeling for the structure like the missile formulation and finite-state aerodynamic modeling for the unsteady aerodynamics, the details of which are given in Ref. [76] and are not repeated here. The structural model is based on the mixed variational formulation for the dynamic of beams developed by Hodges [58]. By discretizing the problem and using simple shape functions, the mixed variational formulation leads to an efficient finite element based solution procedure. Various kinds of forces can be applied to the structure, including follower forces and unsteady aerodynamic forces. The follower force is included in a manner similar to the previous section. The aerodynamic forces are derived from the finite-state aerodynamic model of Peters *et al.* [77], which gives the unsteady aerodynamic forces on an oscillating airfoil. A two-dimensional (2-D) aerodynamic model is used, because the focus here is on wings with high aspect ratio. A 3-D theory may provide higher flutter speeds, making the present results conservative. However, since all the results obtained in the paper use the same 2-D aerodynamic model, the model should be provide adequate predictions of incremental changes of the stability boundary with respect to changes in system parameters. To obtain accurate flutter predictions for wings with low aspect ratio, it would of course be necessary to use a 3-D theory. By coupling the structural and aerodynamic models, one obtains a complete aeroelastic analysis methodology. The full finite element equations are linearized about the static

Table 2: HALE wing data

Half span:	16 m
Chord:	1 m
Mass per unit length:	0.75 kg/m
Moment of Inertia (50% chord):	0.1 kg-m
Spanwise elastic axis:	50% chord
Center of gravity of wing:	50% chord
Bending rigidity (spanwise):	2×10^4N-m^2
Bending rigidity (edgewise):	4×10^6N-m^2
Torsional rigidity	varies with λ
Air density	0.0889 kg/m^3

equilibrium solution, and an eigenvalue analysis is used to determine the stability of the small motions about static equilibrium.

5.3 Results

Results are presented that give insight into the effect of thrust on the flutter characteristics of high-aspect-ratio wings used in high altitude, long endurance (HALE) aircraft. The test case is a flexible high-aspect-ratio wing, and Table 2 gives the properties used in the present work. The engine is located near the tip of the wing. Thus, the test case represents an extreme case in which the effects of thrust are maximized. First, the accuracy of the finite-element analysis is checked against the analytical solution for the thrust-only case. The results are then presented which include both the aerodynamic effects and the thrust follower force. Next, a parametric study investigating the effect of λ on the flutter boundary is presented. Finally, to put the results in perspective, the

Table 3: Data from Feldt and Herrmann

Half span:	4 ft
Chord:	1 ft
Mass per unit length:	0.0132 slug/ft
Moment of inertia (elastic axis):	0.0005346 slug-ft
Spanwise elastic axis:	39% chord
Center of gravity of wing:	42% chord
Bending rigidity:	1638.88 lb-ft^2
Torsional rigidity:	154.17 lb-ft^2
Air density:	0.0011205 slugs/ft^3

thrust required at various trim speeds has been calculated assuming a NACA 0009 airfoil. The thrust required for trim helps in identifying realistic values of the thrust on the wing and thus approximating the percentage change in flutter speed.

5.4 Comparison of Analytical and FE Solutions

Before presenting any finite element results that contain aeroelastic effects, the accuracy of the methodology is first validated against the approximate analytical solution for flutter due to thrust only and against the work of Ref. [54]. For comparison, the follower force is applied at the tip of the wing for $\lambda = 2$. The approximate analytical solution converges with only a few modes. The converged analytical solution, based on 5 bending modes and 3 torsional modes, shows that the critical thrust is 337.2 N. The finite element result using eight elements is 335.1 N, a relative error of 0.6%. This shows that the finite element solution is

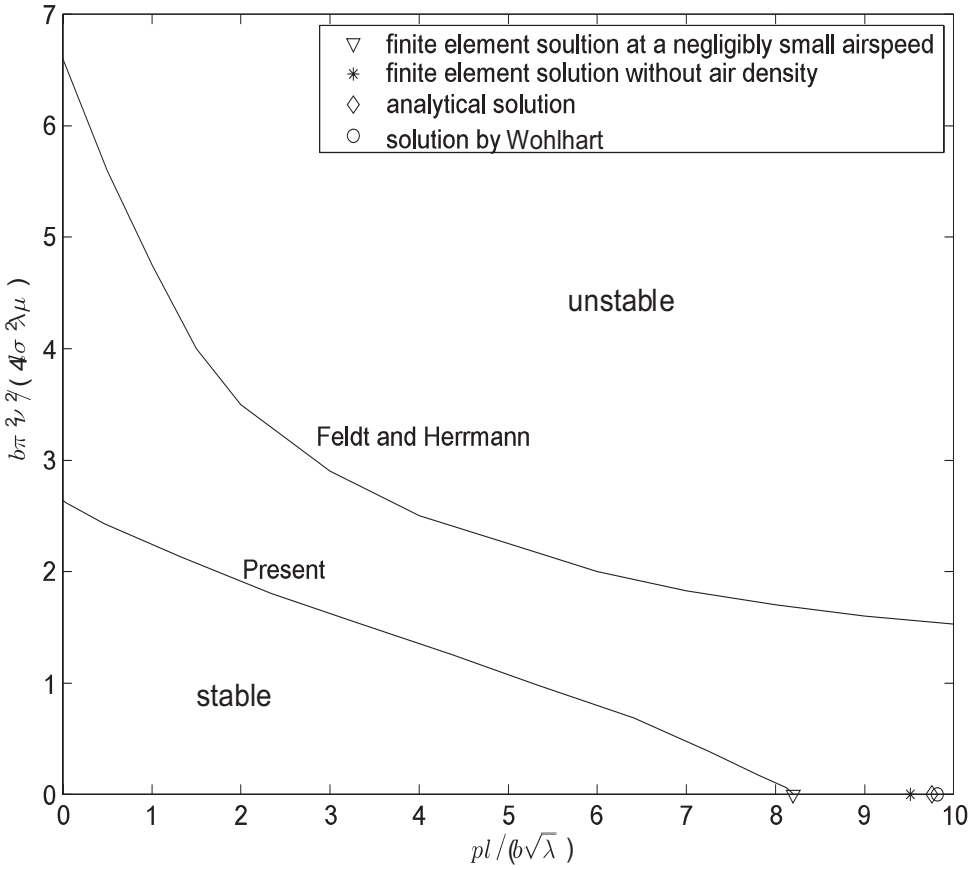

Fig. 16: Comparison with Feldt and Herrmann

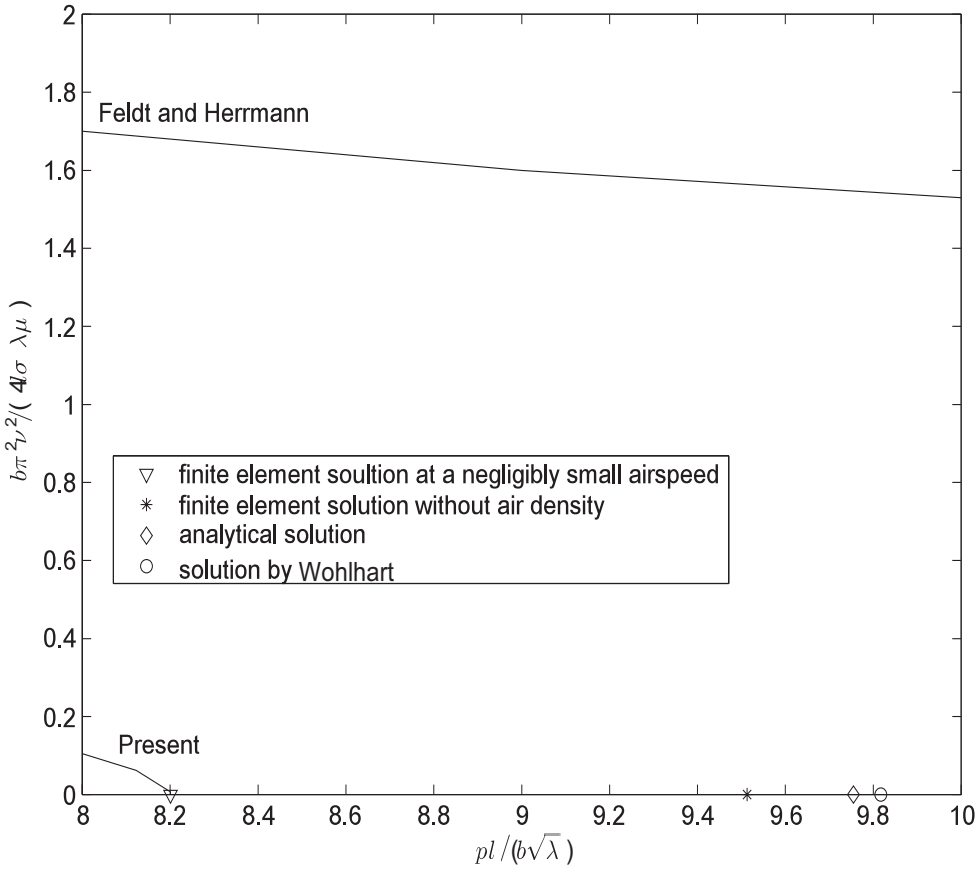

Fig. 17: Comparison with Feldt and Herrmann at very low speed

sufficiently accurate with only eight elements. Moreover, both values agree very well with the analytical solution of Ref. [54].

Next, results from the present analysis are compared with those presented in Ref. [55] for a low-aspect-ratio wing. The data for this test case are given in Table 3. For all cases examined in the absence of aerodynamics, while the present analytical solution, the present finite element solution, and the solution by Ref. [54] all agree quite well, Ref. [55] does not show any flutter instabilities due to thrust only.

The aeroelasticity part of the present finite element methodology was validated in an earlier paper [76]. Unfortunately, as shown in Fig. 16, the results from Ref. [55] do not agree with the present predictions. As discussed above, Ref. [55] does not predict a pure thrust-induced instability while the present analysis does, in agreement with that of Ref. [54]. Even the pure aeroelastic flutter results do not match. Here it should be noted that the ordinate and abscissa are the same as the nondimensional parameters used in Ref. [55], which are expressed in terms of those defined in Eq. 47 and, in addition

$$\begin{aligned} \mu &= \frac{m}{\rho_\infty \pi b^2} \\ v &= \frac{V}{b\omega_{\theta_1}} \end{aligned} \tag{48}$$

where ρ_∞ is the air density, b is the semi-chord, V is the air speed, and ω_{θ_1} is the first uncoupled torsional frequency.

The symbols on Fig. 16, and its more detailed blowup in Fig. 17, represent the finite element solution, the analytical solution, and the solution by Ref. [54]. It is seen that the thrust required for flutter at negligibly small airspeed (crossing

of the flutter boundary curve with the thrust axis) is quite different from that at zero airspeed. The discrepancy is due to two effects. Firstly, the unsteady aerodynamic model predicts forces even at zero airspeed. The forces known as "apparent mass" effects lead to change in the effective mass of the structure and thus change in the dynamics and stability characteristics. The symbol denoting the finite element solution does not include the aerodynamic model (air density in the aerodynamic model is set to zero), so that there are no "apparent mass" terms. That makes this model distinct from one that includes the aerodynamic effects evaluated at a negligibly small airspeed. Secondly, it should be noted that the effect of external damping on the instability of nonconservative systems is quite complex. Even a negligibly small amount of damping has been shown to change the critical force required for instability [78].In the present case, the small airspeed can provide a small damping to change the critical thrust level.

5.5 Change in Flutter Speed with Thrust

The finite element methodology is now used to investigate the effect of thrust on the flutter speed of a cantilevered wing. The thrust is applied at 15 m from the root (*i.e.*, 1 m from the tip of the wing). The flutter boundary is plotted by first selecting a level of thrust, followed by solving the nonlinear steady-state. Once the steady-state solution is obtained, the problem is dynamically linearized about the steady state to get a set of linear equations of motion in terms of the perturbation quantities. The flutter analysis is then conducted to obtain the flutter speed. This presupposes that the airspeed has a weak effect on the

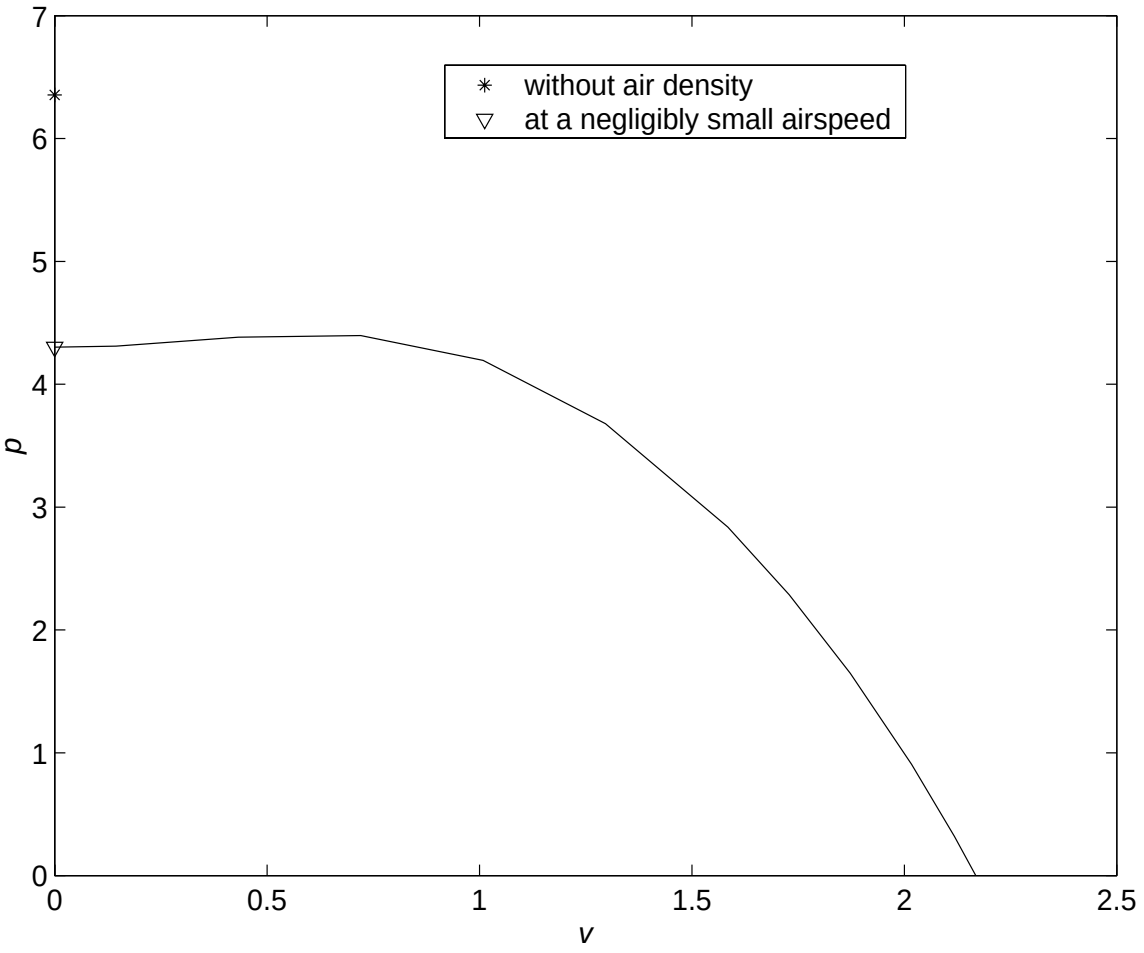

Fig. 18: Flutter boundary for $\lambda = 10$

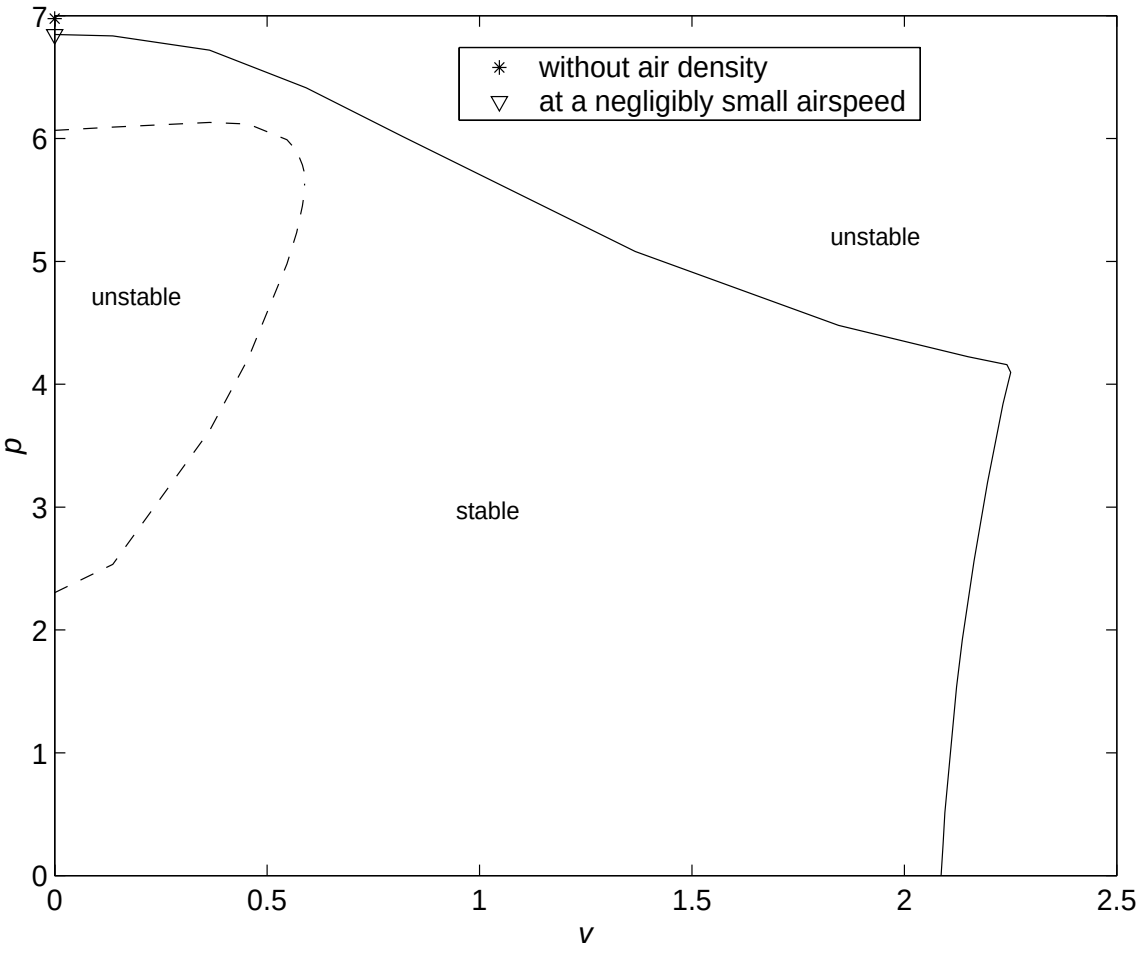

Fig. 19: Flutter boundary for $\lambda = 1$

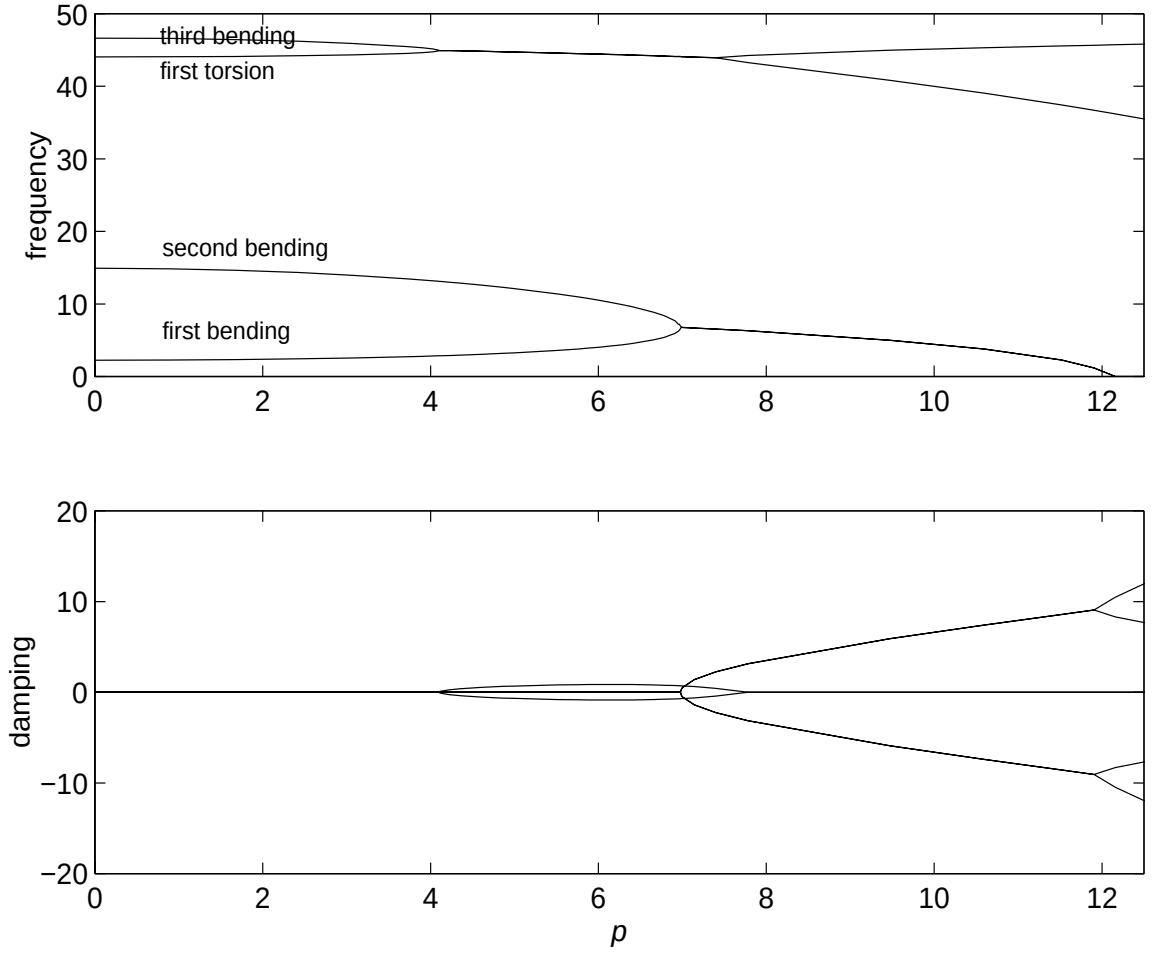

Fig. 20: Frequency and damping at $\lambda = 1$

steady-state solution, which is correct in all cases we examined.

Figure 18 shows the flutter boundary for $\lambda = 10$. All results of the flutter boundary presented from here on are plotted in terms of the nondimensional force p (as defined in Eq. 47), and the standard reduced airspeed v (as defined in Eq. 48). It is seen that there is a continuous decrease in the flutter speed with increase in thrust. From another perspective, one can say that there is a continuous decrease in the magnitude of thrust required for instability with increase in airspeed. This can be qualitatively explained as the addition of the destabilizing effects of the two forces (aerodynamic and follower force) leading to instability at lower levels of the forces. The symbol denoting the finite element solution points out the critical thrust without aerodynamic effects. Again, at zero airspeed there is a jump in flutter force, *i.e.*, a small offset from zero airspeed leads to a sudden decrease of the flutter force. As explained earlier, this is due to the fact that when aerodynamic forces are included, even at zero airspeed, there is a slight shift in the dynamic properties due to the apparent mass of the air and the effect of negligibly small aerodynamic damping.

Excellent agreement was obtained between the finite element and approximate analytical solutions for a wide range of parametric values. The one exception to this is indicated in Fig. 19, which shows the flutter boundary for $\lambda = 1$. The dashed line is a small *unstable* regime predicted by the finite element method that, for reasons unknown, is not predicted by the approximate analytical solution. Figure 20 shows the frequency and damping (imaginary and real part of the eigenvalues) of the system without aerodynamics. It is clear that the unstable

region is due to the coalescence of the first torsion mode with the third bending mode. The frequency of this mode is much higher than the few modes retained in the approximate analytical solution. However, even when a larger number of modes is retained the approximate analytical solution is unable to capture it. Moreover, attempts to link this regime with edgewise flexibility effects also failed. It is clear, however, that a very small amount of structural damping will eliminate this instability, and so it is not of practical importance. Thus, only the low-frequency flutter modes will be considered henceforth.

An important observation can be made from Figs. 18 and 19. Unlike the $\lambda = 10$ case, the critical airspeed for $\lambda = 1$ does not monotonically decrease with an increase in thrust. Rather, there is a reversal. For low levels of thrust, the flutter speed increases, but, as the thrust level is increased further one sees a change in mode of instability from a dominant aeroelastic mode to a dominant follower force instability. Afterwards there is a decrease in the flutter speed with thrust, culminating in the zero speed flutter at the pure follower force instability. To ascertain what is going on here, one needs to vary λ more systematically. The effect of several values of λ on the flutter boundary is shown in Fig. 21. It is seen that the interactions between the thrust and aeroelastic destabilization mechanisms are quite different for lower values of λ (e.g., 1, 1.5, and 2) as compared to the higher values (e.g., 10 and 15). Figure 21 shows these trends changing from one type to the other around $\lambda = 5$. With a careful look at the flutter boundary for $\lambda = 5$, one can see that there is still a range where thrust level increases with airspeed, but it does not show a sudden transition of the flutter frequency as in

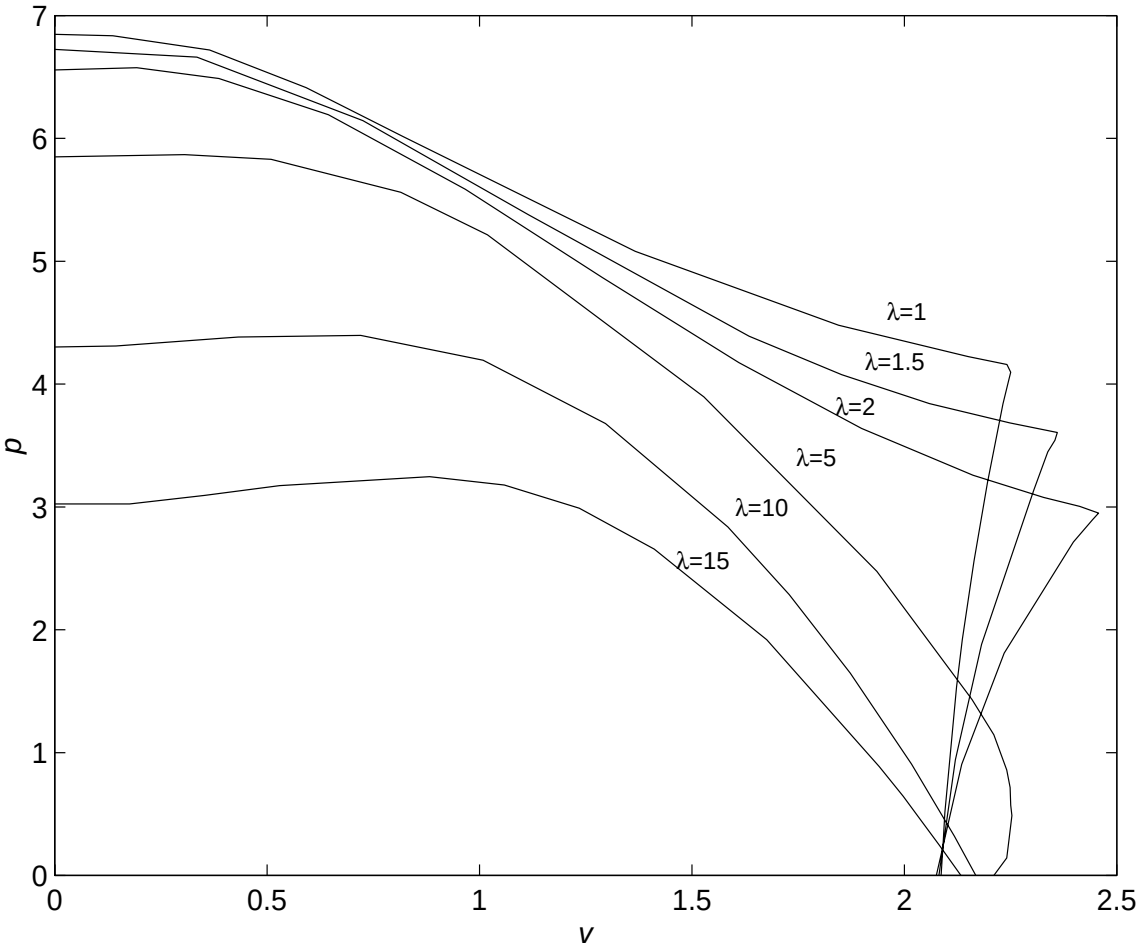

Fig. 21: Effects of λ variation on flutter

the cases where $\lambda < 5$.

5.6 Change in Flutter Speed with λ

To understand the difference in the behavior of the wing at the different λ's, one needs to look at the modes involved in the instability mechanisms. Figure 22 shows the evolution of the pure follower force instability for $\lambda = 2$. For lower λ the

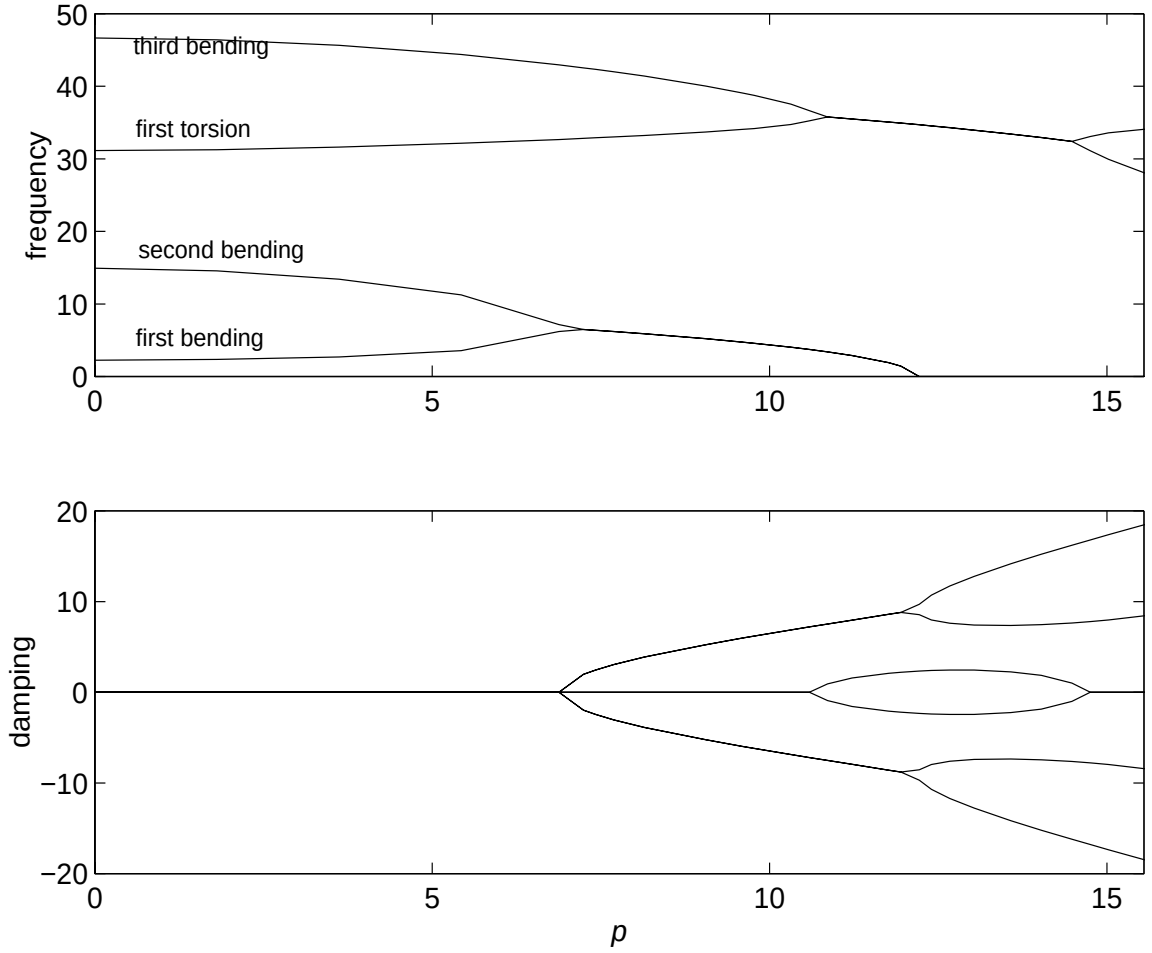

Fig. 22: Eigenanalysis of follower force at $\lambda = 2$

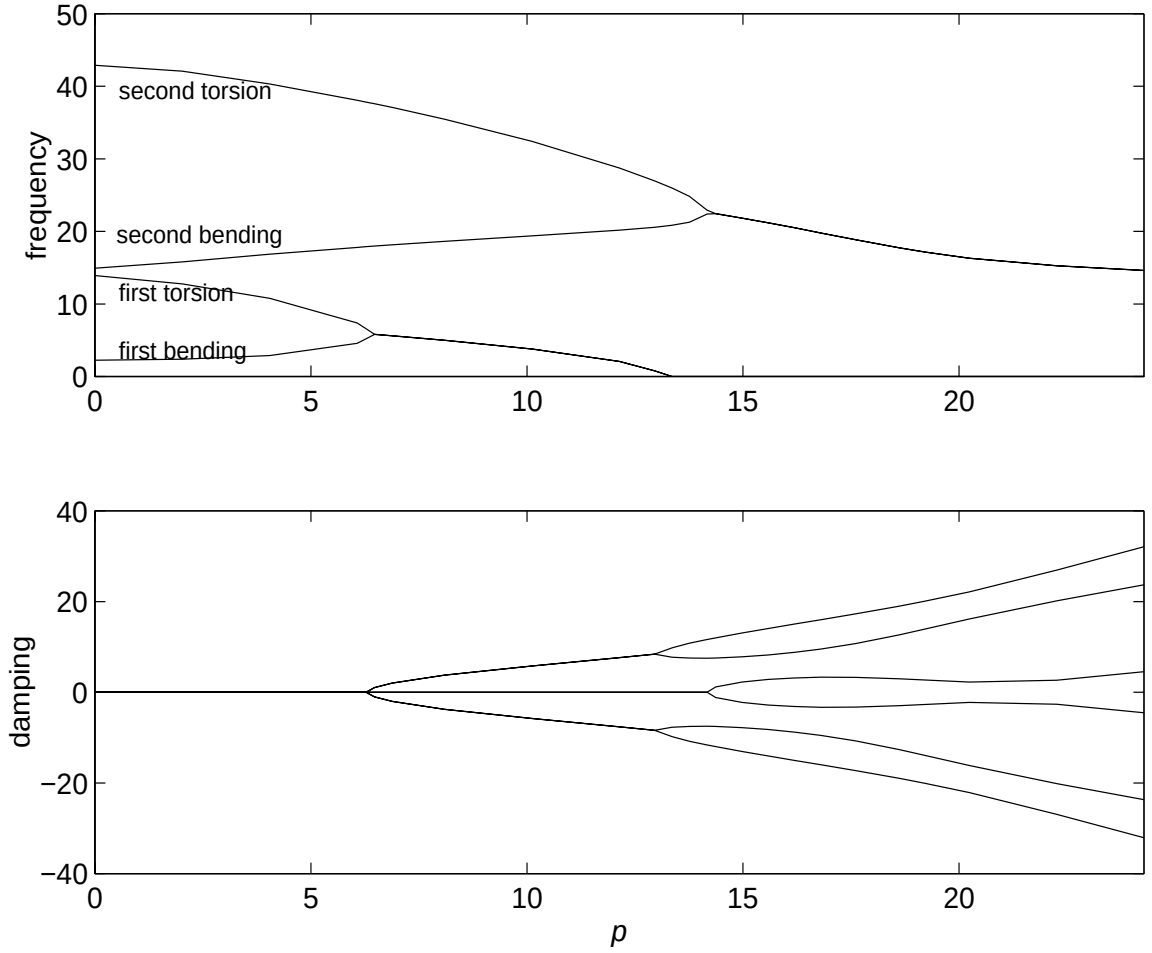

Fig. 23: Eigenanalysis of follower force at $\lambda = 10$

lowest follower-force instability exhibits a bending-bending frequency coalescence. Figure 23 shows a similar plot for $\lambda = 10$, which on the other hand, exhibits an instability due to a torsion-bending frequency coalescence. Modal analysis of pure aeroelastic instabilities show that, in both cases, the pure aeroelastic instabilities come from first torsional modes. The results can be explained qualitatively as follows: Near the aeroelastic flutter speed, the instability for $\lambda = 2$ is less affected by the thrust (than the one for $\lambda = 10$) because different modes are involved in the aeroelastic instability and the follower force instability. For $\lambda = 10$ the torsion-bending instability from pure follower force interacts with the pure aeroelastic torsion instability involving the same modes, thereby decreasing the flutter speed as thrust level increases.

5.7 Trim Solution and Actual Flutter Range

Finally, some points need to be made regarding the levels of thrust on an actual aircraft so as to put the results presented in the earlier sections in the correct perspective. Required thrust to maintain trimmed flight is calculated by assuming a NACA 0009 as the wing airfoil and considering both smooth and "standard" roughness values at the same Reynolds number. The value of roughness affects the drag coefficient significantly [79]. The ratio of total airplane weight to twice the wing panel weight is taken to be either 3 or 6. This is useful in calculating the weight of the aircraft, and thus in estimating the lift and then the drag using the roughness. Here γ is defined as the ratio of fuselage drag over total drag. It

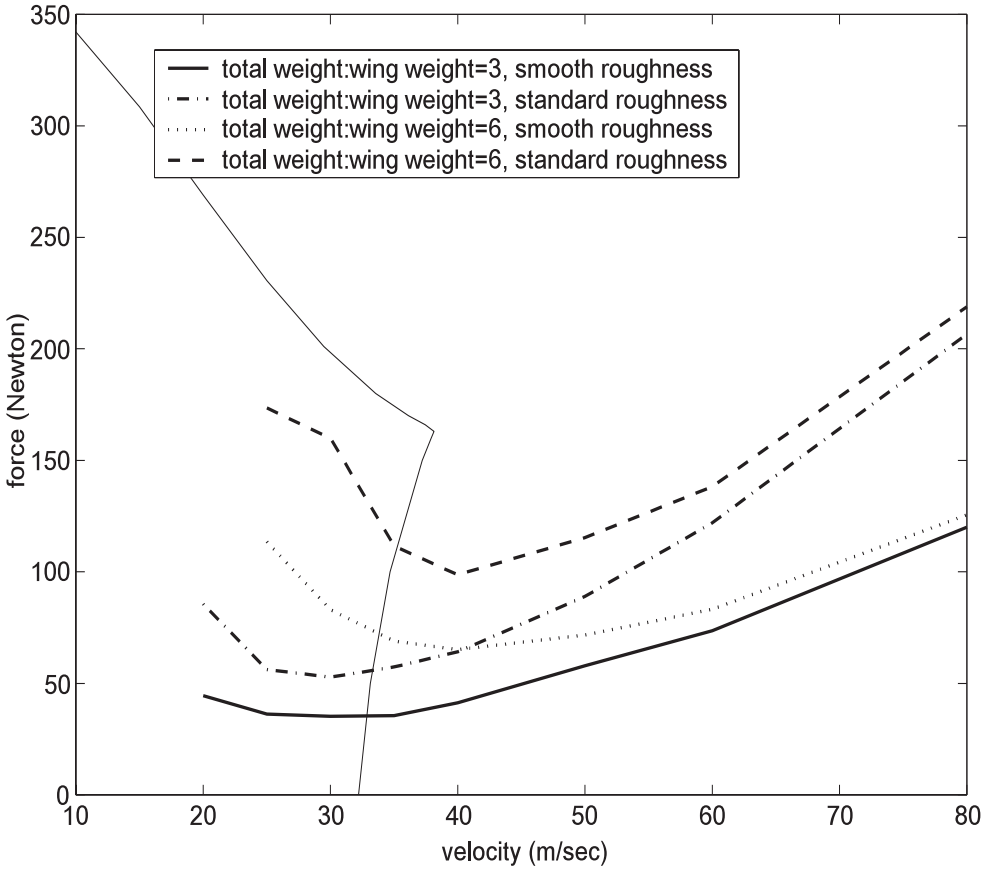

Fig. 24: Flutter range for HALE wing at $\gamma = 0.8$ and $\lambda = 2$

should be noted that the flutter calculation does not make use of γ, *i.e.*, the non-linear drag effects were neglected. γ is used to calculate the total drag (and thus the thrust required) using the wing drag. The wing drag is calculated using the lift to drag ratio for the given smoothness. The lift equal to the total weight is in turn in calculated using the airplane to wing weight ratio. The flutter boundary is shown in Fig. 24 for $\gamma = 0.8$. Also plotted are the velocity-thrust curves for various smoothness and airplane weight factors. The aeroelastic flutter speed without thrust is 32.21 m/s. The flutter speed including the thrust effects for standard roughness and high fuselage mass is 35.8 m/s. Thus, incorporation of thrust can change the predicted flutter speed by 11%. The plots show practical levels of thrust and the corresponding flutter speed for various conditions. In an actual aircraft one would use the thrust levels known for trim flight to estimate the changes in flutter speed.

CHAPTER VI

CONCLUSIONS AND RECOMMENDATIONS

6.1 Conclusions

The effects of follower forces on the aeroelastic behavior of flexible structures have been investigated. Follower forces on their own have been found to greatly affect the instability of flexible structures. Indeed, the well known Beck's problem, a cantilever beam excited by an axially compressive force, is a commonly analyzed problem in the literature. However, free-free beams with axial follower forces and cantilever beams with lateral follower forces have not received as much attention. In aerospace structures, missile thrust and aircraft engine thrust are the typical examples of follower forces. A missile body may become unstable under the action of thrust, and wings may flutter under the influence of transverse thrust alone. Also missile bodies and wings can experience aeroelastic instabilities only caused by aerodynamics during flight. Thus, the combined effects of thrust and aerodynamics naturally lead to the concept of the stability boundary.

The current goal of this research is to investigate the interaction of follower forces with aeroelastic loads along with a study on follower forces themselves. The missile body and wings are modeled in terms of geometrically-exact, nonlinear, beam finite elements. This methodology allows for use of simple shape functions and facilitates time-marching and eigen-analyses. Unsteady missile aerodynamics

and two-dimensional, finite-state wing aerodynamics have been employed to the missile and aircraft wing, respectively. In summary, achievements have been made in the following areas.

6.1.1 Aeroelastic Formulation for Missile Body Stability

In the present effort, the original mixed variational formulation has been modified to include rigid-body dynamics, so that velocity and acceleration can be either specified or left free to vary. Next, the structural formulation is transferred to its weakest form in space and time so that the variables are not differentiated.

It was shown that by removing redundant equations related to some virtual quantities, the total number of system equations and unknowns was greatly reduced. Unless this process is performed, one redundant equation has to be chosen and thrown out. In addition, it gives the relations among interior values.

Aerodynamics loads are based on unsteady-slender body theory and several closed-form aerodynamic theories. The aerodynamic loads include second partial derivatives of certain unknowns, and thus to obtain the weakest form requires integrations by parts. After one time integration by parts, there are still variables with derivatives, which are removed using inverse kinematical relations.

The aeroelastic code is based on combining the aerodynamics and structural formulations. Unlike most eigen-analyses, this time-marching scheme is useful in finding solutions over time. However, if initial conditions are not exactly satisfied among kinematical quantities, the convergence will exhibit sensitivity problems.

6.1.2 Validation and Aeroelastic Studies on Missile Body Flutter

The present code has been validated against several cases, especially the critical load under thrust without directional control. The response is divergent for values of thrust far above the critical value given in the literature. However, near the critical value, whether the thrust was high or low, limit cycles were observed.

As with general aircraft, velocity is an important aerodynamic element related to missile aeroelastic instability. As the flight speed increases, so does the amplitude of perturbed deflection. This result indicates that the aerodynamics serve to decrease the effective stiffness of the missile.

Missile body stiffness, along with velocity, greatly affects missile stability. A prediction of stable rigid-body motion does not necessarily guarantee the stability of highly flexible structures like missiles with a high fineness ratio. With an increase in velocity, the center of pressure of the missile was shown to approach the center of mass. Depending on the missile and flight conditions, it is possible that the flexible static margin would be negative. Thus, a designer would have to find such a flexible static margin at the early design phase to avoid structural failure.

The stability boundaries were obtained for certain bending stiffnesses. The response, at points far outside the stability boundary, was shown to be divergent. As expected, the response was bounded or convergent inside the boundary over time. It can be seen from the current results that highly flexible missiles such as ballistic missiles should be carefully designed to avoid aeroelastic instability.

6.1.3 Aeroelastic Studies of Wing Mounted Engine

Finite-state aerodynamics is employed to calculate unsteady aerodynamics. The structural model is based on a mixed variational formulation. Coupling of these two models leads to a complete aeroelastic analysis methodology. Linearization of the coupled equations about the static equilibrium solution is taken and an eigenvalue analysis is performed to determine the stability of small motion from the static equilibrium.

An analytical solution for the *in vacuo* case was developed and shown to closely match results from the numerical method. A parametric study of thrust effects on aeroelastic flutter was performed. Whether or not thrust is stabilizing depends strongly on λ, the ratio of bending stiffness to torsional stiffness. For $\lambda \leq 5$, it was shown that thrust up to a certain value can increase flutter speed. For $\lambda \geq 10$, thrust always decreases flutter speed. Moreover, the shape of flutter curve is greatly affected by λ. The reasons that flutter curve changed according to the different λ values were explained by using the mode shape interactions.

Flutter analysis was performed for the trimmed flight with NACA 0009 as a wing airfoil. The thrust required to maintain the trim condition was calculated at various speeds. Incorporation of thrust with aerodynamics was shown to change the flutter speed by 11% when $\lambda = 2$.

6.2 Recommendations

The structural and aerodynamic formulations have been combined to give a complete dynamic and aeroelastic analysis of flying missiles. With some additions

to this tool, investigations of a wide variety of dynamic and aeroelastic stability phenomena can be undertaken over a wide range of steady flight conditions, including spin and thrust in the present analysis. As one of the ways to stabilize the directional control, spinning is used. When spinning speed increases, the stabilization effect increases based on the rigid-body model. In the flexible model, however, the stability region is known to vary. The aeroelastic effects of spin are not well understood.

The work performed on the missile body aeroelasticity with a follower force is related to a rectilinear flight with a zero rigid-body angle of attack. The result verified the interaction of thrust and aerodynamic force. Generally, missiles experience a small angle of attack during powered flight and a high angle of attack during a maneuvering flight. A high angle-of-attack analysis would require a much more refined aerodynamic theory.

The current formulation does not include the mass variation effect. To see more clearly the dynamic response and stability issues during powered flight, treatment of mass variation according to fuel consumption will be needed. In addition, mass distribution along with bending stiffness is known to significantly change the critical load associated with a follower force. Much research on the effect of concentrated mass and its location on the stability has been performed for the flexible system subjected to a compressive follower force. However, there is currently no closed form or analytical optimization method. Thus, it will be of interest to investigate the mass effect on stability problems.

Possible coupling between the flight mechanics (i.e., trajectory optimization,

constraints, etc.) and the aeroelasticity (including internal loads and stability) has yet to be approached. For example, turning ability can be quantified in terms of internal loads, and the applicability of the corresponding simplistic constraint (the so-called q-α constraint) imposed in trajectory optimization can be examined in this broader context. The present analysis is not sufficiently computationally efficient to undertake such a study at this time. However, with additional attention devoted to efficiency and with faster computers in the future, such a study should become more feasible.

Finally, the current flutter analysis based on eigenvalue analysis considered only the thrust of a wing-mounted engine. But in reality, engine mass, engine inertia and engine gyroscopic effects might affect system stability. Also, the effect of the location of the engine at different points along the wing needs to be investigated on the flutter boundary.

APPENDIX A

DERIVATIONS

A.1 Eq. (12)

To derive $\delta v_o = \delta\dot{q}_o + \widetilde{\omega}_o \delta q_o + \widetilde{v}_o \delta\psi_o$

Starting from $v_o = C_o \dot{u}_o$ and $\widetilde{\delta\psi}_o = -\delta C_o C_o^T$

$\delta v_o = \delta C_o \dot{u}_o + C_o \delta\dot{u}_o$

$C_o \delta u_o = \delta q_o$

$\delta C_o \dot{u}_o = \delta C_o C_o^T v_o = -\widetilde{\delta\psi}_o v_o = \widetilde{v}_o \delta\psi_o$

$\delta\dot{q}_o = \dot{C}_o \delta u_o + C_o \delta\dot{u}_o$

$C_o \delta\dot{u}_o = \delta\dot{q}_o - \dot{C}_o C_o^T \delta q_o = \delta\dot{q}_o + \widetilde{\omega}_o \delta q_o$

This proves Eq. (12).

A.2 Eq. (13)

To derive $\delta\omega_o = \delta\dot{\psi}_o + \widetilde{\omega}_o \delta\psi_o$

Starting from $\widetilde{\omega}_o = -\dot{C}_o C_o^T$ and $\widetilde{\delta\psi}_o = -\delta C_o C_o^T$

$\widetilde{\delta\dot{\psi}}_o = -\delta\dot{C}_o C_o^T - \delta C_o \dot{C}_o^T$

Then,

$$\begin{aligned}\widetilde{\delta\omega}_o &= -\delta\dot{C}_o C_o^T - \dot{C}_o \delta C_o^T = \widetilde{\delta\dot{\psi}}_o + \delta C_o \dot{C}_o^T - \dot{C}_o \delta C_o^T \\ &= \widetilde{\delta\dot{\psi}}_o + \delta C_o C_o^T C_o \dot{C}_o^T - \dot{C}_o C_o^T C_o \delta C_o^T \\ &= \widetilde{\delta\dot{\psi}}_o - \widetilde{\delta\psi}_o \widetilde{\omega}_o + \widetilde{\omega}_o \widetilde{\delta\psi}_o \\ &= \widetilde{\delta\dot{\psi}}_o + \widetilde{\omega}_o \widetilde{\delta\psi}_o - \widetilde{\delta\psi}_o \widetilde{\omega}_o\end{aligned}$$

If $\widetilde{\ }$ is removed on both sides of the above equation, $\delta\omega_o = \delta\dot{\psi}_o + \widetilde{\omega}_o \delta\psi_o$ is obtained.

A.3 Eq. (14)

$$\begin{aligned}\delta G =& \delta q_o^T C_o \int_0^\ell mge_3 dx_1 - \delta\psi_o^T \widetilde{C_o e_3} \int_0^\ell mg(r_b + u_b + C^T\xi_B) dx_1 \\ &+ \int_0^\ell \overline{\delta q}_B^T C C_o e_3 mg dx_1 + \int_0^\ell \overline{\delta\psi}_B^T \widetilde{\xi}_B C C_o e_3 mg dx_1\end{aligned}$$

Starting from $G = \int_0^\ell mge_3^T(u_o + C_o^T(r_b + u_b + C^T\xi_B))dx_1$ and taking virtual variation,

$$\delta G = \int_0^l mge_3^T[C_o^T\delta q_o + C_o^T\widetilde{\delta\psi}_o(r_b + u_b + C^T\overline{\xi}_B) + C_o^T C^T\overline{\delta q}_B + C_o^T C^T\widetilde{\overline{\delta\psi}}_B\overline{\xi}_B]dx_1$$

$$\begin{aligned}& e_3^T C_o^T \delta q_o = \delta q_o^T C_o e_3 \\ & e_3^T C_o^T \widetilde{\delta\psi}_o (r_b + u_b + C^T\overline{\xi}_B) = -(r_b + u_b + C^T\overline{\xi}_B)^T \widetilde{\delta\psi}_o C_o e_3 \\ & = \widetilde{\delta\psi}_o^T (r_b + \widetilde{u_b + C^T\overline{\xi}_B}) C_o e_3 = -\delta\psi_o^T \widetilde{C_o e_3}(r_b + u_b + C^T\overline{\xi}_B) \\ & e_3^T C_o^T C^T \overline{\delta q}_B = \overline{\delta q}_B^T C C_o e_3 \\ & e_3^T C_o^T C^T \widetilde{\overline{\delta\psi}}_B \overline{\xi}_B = -\overline{\xi}_B^T \widetilde{\overline{\delta\psi}}_B C C_o e_3 = \overline{\delta\psi}_B^T \widetilde{\overline{\xi}}_B C C_o e_3\end{aligned}$$

This completes the derivation.

APPENDIX B

DISTRIBUTED FORCE

The distributed normal force acts along the missile body, and also contributes to the rigid body forces. The way of getting system equations for the elastic virtual quantity $\overline{\delta q}_B$ is explained. To conduct finite element discretization for the distributed force, integration by parts should be first performed to reduce order of the variables.

$$
\begin{aligned}
&\int_{t_1}^{t_2}\int_0^l \overline{\delta q}_B^T f_B dt = -\int_{t_1}^{t_2}\int_0^l \overline{\delta q}_B^T C^{BW} f_W dx dt \\
&= -\int_{t_1}^{t_2}\int_0^l \overline{\delta q}_B^T C^{BW}(\rho_\infty v_o^2 \tfrac{dS}{dx}\tfrac{\partial\lambda}{\partial x} + \rho_\infty v_o \tfrac{dS}{dx}\tfrac{\partial\lambda}{\partial t} + \rho_\infty v_o^2 S\tfrac{\partial^2\lambda}{\partial x^2} + 2\rho_\infty v_o S\tfrac{\partial^2\lambda}{\partial x\partial t} + \rho_\infty S\tfrac{\partial^2\lambda}{\partial t^2})dxdt \\
&= -\int_{t_1}^{t_2}\int_0^l \left\{ \begin{array}{l} \overline{\delta q}_B^T C^{BW}(\rho_\infty v_o^2 \tfrac{dS}{dx}\tfrac{\partial\lambda}{\partial x} + \rho_\infty v_o \tfrac{dS}{dx}\tfrac{\partial\lambda}{\partial t}) \\ -(\overline{\delta q}'^T_B C^{BW} S + \overline{\delta q}_B^T C'^{BW} S + \overline{\delta q}_B^T C^{BW}\tfrac{dS}{dx})\rho_\infty v_o^2\tfrac{\partial\lambda}{\partial x} \\ -(\overline{\delta q}'^T_B C^{BW} S + \overline{\delta q}_B^T C'^{BW} S + \overline{\delta q}_B^T C^{BW}\tfrac{dS}{dx})2\rho_\infty v_o\tfrac{\partial\lambda}{\partial t} \end{array} \right\} dxdt \\
&+ \int_{t_1}^{t_2}\int_0^l (\overline{\delta\dot{q}}_B^T C^{BW} + \overline{\delta q}_B^T \dot{C}^{BW})\rho_\infty S\tfrac{\partial\lambda}{\partial t}dxdt \\
&- \int_{t_1}^{t_2} \overline{\delta q}_B^T C^{BW} S\ (\rho_\infty v_o^2\tfrac{\partial\lambda}{\partial x} + 2\rho_\infty v_o\tfrac{\partial\lambda}{\partial t})\big|_o^l\, dt \\
&- \int_0^l \overline{\delta q}_B^T C^{BW} S\ \tfrac{\partial\lambda}{\partial t}\big|_{t_1}^{t_2} dx
\end{aligned}
$$

To be continued from the previous page

$$= \int_{t_1}^{t_2}\int_0^l \overline{\delta q}_B^T \left\{ (C^{BW}\tfrac{dS}{dx} + 2C'^{BW}S)\rho_\infty v_o \tfrac{\partial\lambda}{\partial t} + C'^{BW}\rho_\infty v_o^2 S\tfrac{\partial\lambda}{\partial x} + \dot{C}^{BW}\rho_\infty S\tfrac{\partial\lambda}{\partial t} \right\} dxdt$$
$$+ \int_{t_1}^{t_2}\int_0^l \overline{\delta q'}_B^T \left\{ C^{BW}\rho_\infty v_o^2 S\tfrac{\partial\lambda}{\partial x} + 2C^{BW}\rho_\infty v_o S\tfrac{\partial\lambda}{\partial t} \right\} dxdt$$
$$+ \int_{t_1}^{t_2}\int_0^l \overline{\delta \dot{q}}_B^T (C^{BW}\rho_\infty S\tfrac{\partial\lambda}{\partial t}) dxdt$$
$$- \int_{t_1}^{t_2} \overline{\delta q}_B^T \left(C^{BW}\rho_\infty v_o^2 S\tfrac{\partial\lambda}{\partial x} + 2C^{BW}\rho_\infty v_o S\tfrac{\partial\lambda}{\partial t}\right)\Big|_o^l dt$$
$$- \int_0^l \overline{\delta q}_B^T (C^{BW}\rho_\infty\ S\tfrac{\partial\lambda}{\partial t})\Big|_{t_1}^{t_2} dx$$

If we set

$$\{A\} = (C^{BW}\tfrac{dS}{dx} + 2C'^{BW}S)\rho_\infty v_o \tfrac{\partial\lambda}{\partial t} + C'^{BW}\rho_\infty v_o^2 S\tfrac{\partial\lambda}{\partial x} + \dot{C}^{BW}\rho_\infty S\tfrac{\partial\lambda}{\partial t}$$
$$\{B\} = C^{BW}\rho_\infty v_o^2 S\tfrac{\partial\lambda}{\partial x} + 2C^{BW}\rho_\infty v_o S\tfrac{\partial\lambda}{\partial t}$$
$$\{D\} = C^{BW}\rho_\infty S\tfrac{\partial\lambda}{\partial t}$$

where

$C'^{BW} \simeq -\widetilde{\kappa}C^{bW}$,

$\dot{C}^{BW} \simeq [-\widetilde{\Omega}_B(\Delta - \widetilde{\theta}) + (\Delta - \widetilde{\theta})\widetilde{\omega}_o]C^{bW} - (\Delta - \widetilde{\theta})\widetilde{\omega}_o C^{bW} + (\Delta - \widetilde{\theta})C_o C^{IW}\widetilde{\omega}^{WI}$

The above equation leads to the following form

$$= \int_{t_1}^{t_2}\int_0^l \overline{\delta q}_B^T\{A\}dxdt$$
$$+ \int_{t_1}^{t_2}\int_0^l \overline{\delta q'}_B^T\{B\}dxdt$$
$$+ \int_{t_1}^{t_2}\int_0^l \overline{\delta \dot{q}}_B^T\{D\}dxdt$$
$$- \int_{t_1}^{t_2} \overline{\delta q}_B^T\{\ B\}\Big|_o^l dt$$
$$- \int_0^l \overline{\delta q}_B^T\{\ D\}\Big|_{t_1}^{t_2} dx$$

And finally the shape function for $\overline{\delta q}_B$ and the expressions for $\frac{\partial\lambda}{\partial t}$ and $\frac{\partial\lambda}{\partial x}$ are substituted in the above equation to get the system equations for the elastic virtual quantity $\overline{\delta q}_B$. At the coding, intermediate values $\frac{\partial\lambda}{\partial t}$ and $\frac{\partial\lambda}{\partial x}$ are defined for simplification.

APPENDIX C

RIGID-BODY FORCE AND MOMENT FROM DISTRIBUTED FORCE

C.1 rigid-body force from running mass part

The distributed normal force contributes to the rigid-body force at the reference point. The way of getting system equations for the virtual quantity δq_o due to the distributed force is explained.

$$
\begin{aligned}
&\textstyle\int_{t_1}^{t_2} \delta q_o^T f_o dt = \int_{t_1}^{t_2} \delta q_o^T \int_0^l C^T f_B dx dt \\
&= \textstyle\int_{t_1}^{t_2} \delta q_o^T C^{bW} \int_0^l f_w dx dt \\
&= -\textstyle\int_{t_1}^{t_2} \delta q_o^T C^{bW} \int_0^l (\rho_\infty v_o^2 \frac{dS}{dx}\frac{\partial \lambda}{\partial x} + \rho_\infty v_o \frac{dS}{dx}\frac{\partial \lambda}{\partial t} + \rho_\infty v_o^2 S\frac{\partial^2 \lambda}{\partial x^2} + 2\rho_\infty v_o S\frac{\partial^2 \lambda}{\partial x \partial t} + \rho_\infty S\frac{\partial^2 \lambda}{\partial t^2}) dx dt \\
&= -\textstyle\int_{t_1}^{t_2} \delta q_o^T C^{bW} \int_0^l (\rho_\infty v_o^2 \frac{dS}{dx}\frac{\partial \lambda}{\partial x} + \rho_\infty v_o \frac{dS}{dx}\frac{\partial \lambda}{\partial t} - \rho_\infty v_o^2 \frac{dS}{dx}\frac{\partial \lambda}{\partial x} - 2\rho_\infty v_o \frac{dS}{dx}\frac{\partial \lambda}{\partial t}) dx dt \\
&+ \textstyle\int_{t_1}^{t_2} (\delta \dot{q}_o^T C^{bW} + \delta q_o^T \dot{C}^{bW}) \int_0^l \rho_\infty S\frac{\partial \lambda}{\partial t} dx dt \\
&- \textstyle\int_{t_1}^{t_2} \delta q_o^T C^{bW} \ (\rho_\infty v_o^2 S\frac{\partial \lambda}{\partial x} + 2\rho_\infty v_o S\frac{\partial \lambda}{\partial t})\big|_o^l dt \\
&- \textstyle\int_0^l \delta q_o^T C^{bW} \rho_\infty \ S\frac{\partial \lambda}{\partial t}\big|_{t_1}^{t_2} dx \\
&= \textstyle\int_{t_1}^{t_2} \delta q_o^T C^{bW} \int_0^l (\rho_\infty v_o \frac{dS}{dx}\frac{\partial \lambda}{\partial t}) dx dt + \int_{t_1}^{t_2} (\delta \dot{q}_o^T C^{bW} + \delta q_o^T \dot{C}^{bW}) \int_0^l \rho_\infty S\frac{\partial \lambda}{\partial t} dx dt \\
&- \textstyle\int_{t_1}^{t_2} \delta q_o^T C^{bW} \ (\rho_\infty v_o^2 S\frac{\partial \lambda}{\partial x} + 2\rho_\infty v_o S\frac{\partial \lambda}{\partial t})\big|_o^l dt \\
&- \textstyle\int_0^l \delta q_o^T C^{bW} \rho_\infty \ S\frac{\partial \lambda}{\partial t}\big|_{t_1}^{t_2} dx
\end{aligned}
$$

The shape functions of δq_o and the expressions for $\frac{\partial \lambda}{\partial t}$ and $\frac{\partial \lambda}{\partial x}$ are substituted into the final form, and after discretization over the beam length, the system equations for rigid-body virtual quantity δq_o due to distributed running mass effect are obtained.

C.2 rigid-body moment from distributed force

The distributed normal force contributes to the rigid-body moment about the reference point. The way of getting system equations for the virtual quantity $\delta\psi_o$ due to the distributed force is explained.

$$
\begin{aligned}
&\textstyle\int_{t_1}^{t_2} \delta\psi_o^T f_o dt = \int_{t_1}^{t_2} \delta\psi_o^T \int_0^l (\widetilde{r} + \widetilde{u}_b) C^T f_B dx dt \\
&= \textstyle\int_{t_1}^{t_2} \delta\psi_o^T C^{bW} \int_0^l (\widetilde{r} + \widetilde{u}_b) f_w dx dt \\
&= -\textstyle\int_{t_1}^{t_2} \delta\psi_o^T C^{bW} \int_0^l (\widetilde{r} + \widetilde{u}_b) \left\{ \begin{array}{l} \rho_\infty v_o^2 \frac{dS}{dx}\frac{\partial\lambda}{\partial x} + \rho_\infty v_o \frac{dS}{dx}\frac{\partial\lambda}{\partial t} + \\ \rho_\infty v_o^2 S \frac{\partial^2\lambda}{\partial x^2} + 2\rho_\infty v_o S \frac{\partial^2\lambda}{\partial x \partial t} + \rho_\infty S \frac{\partial^2\lambda}{\partial t^2} \end{array} \right\} dx dt \\
&= -\textstyle\int_{t_1}^{t_2} \delta\psi_o^T C^{bW} \int_0^l (\widetilde{r} + \widetilde{u}_b) \left\{ \rho_\infty v_o^2 \frac{dS}{dx}\frac{\partial\lambda}{\partial x} + \rho_\infty v_o \frac{dS}{dx}\frac{\partial\lambda}{\partial t} \right\} dx dt \\
&+ \textstyle\int_{t_1}^{t_2} \delta\psi_o^T C^{bW} \int_0^l \left\{ (\widetilde{e}_1 + \widetilde{u}_b') \rho_\infty v_o^2 S \frac{\partial\lambda}{\partial x} + (\widetilde{r} + \widetilde{u}_b) \rho_\infty v_o^2 \frac{dS}{dx}\frac{\partial\lambda}{\partial x} \right\} dx dt \\
&+ \textstyle\int_{t_1}^{t_2} \delta\psi_o^T C^{bW} \int_0^l \left\{ 2(\widetilde{e}_1 + \widetilde{u}_b') \rho_\infty v_o S \frac{\partial\lambda}{\partial t} + 2(\widetilde{r} + \widetilde{u}_b) \rho_\infty v_o \frac{dS}{dx}\frac{\partial\lambda}{\partial t} \right\} dx dt \\
&+ \textstyle\int_{t_1}^{t_2} (\delta\dot{\psi}_o^T C^{bW} + \delta\psi_o^T \dot{C}^{bW}) \int_0^l (\widetilde{r} + \widetilde{u}_b) \rho_\infty S \frac{\partial\lambda}{\partial t} dx dt + \int_{t_1}^{t_2} \delta\psi_o^T C^{bW} \int_0^l \ddot{\widetilde{u}}_b \rho_\infty S \frac{\partial\lambda}{\partial t} dx dt \\
&- \textstyle\int_{t_1}^{t_2} \delta\psi_o^T C^{bW} (\widetilde{r} + \widetilde{u}_b) \left(\rho_\infty v_o^2 S \frac{\partial\lambda}{\partial x} + 2\rho_\infty v_o S \frac{\partial\lambda}{\partial t} \right)\Big|_o^l dt \\
&- \textstyle\int_0^l \delta\psi_o^T C^{bW} (\widetilde{r} + \widetilde{u}_b) \rho_\infty \, S \frac{\partial\lambda}{\partial t}\Big|_{t_1}^{t_2} dx \\
&= \textstyle\int_{t_1}^{t_2} \delta\psi_o^T C^{bW} \int_0^l \left\{ (\widetilde{r} + \widetilde{u}_b) \rho_\infty v_o \frac{dS}{dx}\frac{\partial\lambda}{\partial t} + 2(\widetilde{e}_1 + \widetilde{u}_b') \rho_\infty v_o S \frac{\partial\lambda}{\partial t} + (\widetilde{e}_1 + \widetilde{u}_b') \rho_\infty v_o^2 S \frac{\partial\lambda}{\partial x} \right\} dx dt \\
&+ \textstyle\int_{t_1}^{t_2} (\delta\dot{\psi}_o^T C^{bW} + \delta\psi_o^T \dot{C}^{bW}) \int_0^l (\widetilde{r} + \widetilde{u}_b) \rho_\infty S \frac{\partial\lambda}{\partial t} dx dt + \int_{t_1}^{t_2} \delta\psi_o^T C^{bW} \int_0^l \ddot{\widetilde{u}}_b \rho_\infty S \frac{\partial\lambda}{\partial t} dx dt \\
&- \textstyle\int_{t_1}^{t_2} \delta\psi_o^T C^{bW} (\widetilde{r} + \widetilde{u}_b) \left(\rho_\infty v_o^2 S \frac{\partial\lambda}{\partial x} + 2\rho_\infty v_o S \frac{\partial\lambda}{\partial t} \right)\Big|_o^l dt \\
&- \textstyle\int_0^l \delta\psi_o^T C^{bW} (\widetilde{r} + \widetilde{u}_b) \rho_\infty \, S \frac{\partial\lambda}{\partial t}\Big|_{t_1}^{t_2} dx
\end{aligned}
$$

The shape functions of $\delta\psi_o$ and the expressions for $\frac{\partial\lambda}{\partial t}$ and $\frac{\partial\lambda}{\partial x}$ are substituted into the final form, the system equations for the rigid-body virtual quantity $\delta\psi_o$ due to the unsteady normal force distribution are obtained.

REFERENCES

[1] Beal, T. R., "Dynamic Stability of a Flexible Missile under Constant and Pulsating Thrusts," *AIAA Journal*, Vol. 3, No. 3, March 1965, pp. 486 – 494.

[2] Peters, D. A. and Wu, J. J., "Asymptotic Solutions to a Stability Problem," *Journal of Sound and Vibration*, Vol. 59, No. 4, 1978, pp. 591 – 610.

[3] Wu, J. J., "Missile Stability Using Finite Elements – an Unconstrained Variational Approach," *American Institute of Aeronautics and Astronautics Journal*, Vol. 14, 1976, pp. 313–319.

[4] Park, Y. P. and Mote, Jr., C. D., "The Maximum Controlled Follower Force on a Free-Free Beam Carrying a Concentrated Mass," *Journal of Sound and Vibration*, Vol. 98, No. 2, 1985, pp. 247 – 256.

[5] Kirillov, O. N. and Seyranian, A. P., "Optimization of Stability of a Flexible Missile under Follower Thrust," AIAA Paper 98-4969, Sept 1998.

[6] Park, Y. P., "Dynamic Stability of a Free Timoshenko Beam Under a Controlled Follower Force," *Journal of Sound and Vibration*, Vol. 113, No. 3, March 1987, pp. 407 – 415.

[7] Sugiyama, Y., Katayama, K., and Kinoi, S., "Flutter of Cantilevered Column under Rocket Thrust," *Journal of Aerospace Engineering*, Vol. 8, No. 1, Jan. 1995, pp. 9–15.

[8] Kim, J.-H. and Choo, Y.-S., "Dynamic Stability of a Free-free Timoshenko beam subjected to a Pulsating follower force," *Journal of Sound and Vibration*, Vol. 216, No. 4, Oct. 1998, pp. 623 – 636.

[9] Yoon, S. J. and Kim, J. H., "A Concentrated Mass on the Spinning Unconstrained Beam Subjected to a Thrust," *Journal of Sound and Vibration*, Vol. 254, No. 4, 2002, pp. 621–634.

[10] Leipholz, H. H. E. and Piche, R., "Stability of Follower-Force Rods with Weight," *Journal of Engineering Mechanics*, Vol. 110, No. 3, March 1984, pp. 367–379.

[11] Foweler, R. H., Gallop, J. L., Lock, C. N., and Richmond, H. W., "Aerodynamics of a Spinning shell," *Philosophical Transactions of Royal Society of London (A)*, Vol. 221, 1920, pp. 295 – 387.

[12] Mcshane, E., Kelley, J. L., and Reno, F., *Exterior Ballistics*, University of Denver Press, Denver, CO, 1953.

[13] Nicolaides, J. D., "On the Free Flight Motion of Missiles Having Slight Configurational Asymmetries," Tech. Rep. BRL Rep. 858, U.S. Army Ballistic Research Laboratories, 1953.

[14] Platus, D. H., "Ballistic Re-entry Vehicle Flight Dynamics," *Journal of Guidance and Control*, Vol. 5, Jan.-Feb. 1982, pp. 4 – 16.

[15] Nicolaides, J. D., "Two Non-linear Problems in the Flight Dynamics of Modern Ballistic Missiles," *Institute of Aeronautical Sciences*, 1959, Paper 59-17.

[16] Murphy, C. H., "Free Flight Motion of Missiles of Symmetric Missiles," Tech. Rep. BRL-TR-1216, U.S. Army Ballistic Research Laboratories, Aberdeen Proving Ground, MD, 1963.

[17] Clare, T. A., "Resonace Instability for Finned Configurations Having Nonlinear Properties," *Journal of Spacecraft and Rockets*, Vol. 8, March 1971, pp. 278–283.

[18] Pepitone, T. R. and Jacobson, I. D., "Resonant Behavior of a Symmetric Missile Having Roll Orientation-Dependent Aerodynamics," *Journal of Guidance and Control*, Vol. 1, Sep.-Oct. 1978, pp. 335–339.

[19] Murphy, C. H., "Symmetric Missile Dynamic Instabilities," *Journal of Guidance and Control*, Vol. 4, No. 1, Sep.-Oct. 1981, pp. 464 – 471.

[20] Murphy, C. H., "Side Moment Exerted by a Spinning, Coning, Highly Viscous Liquid Payload," Tech. Rep. BRL-TR-3074, U.S. Army Ballistic Research Laboratory, Aberdeen Proving Ground, MD, 1989.

[21] Vahdati, M. Kurt-Elli, H. and Imregun, M., "Missile fin flutter analysis using an integrated aeroelasticity method," *CEAS International Forum on Aeroelasticity and Structural Dynamics*, Associazione Italiana di Aeronautica ed Astronautica, Rome, June 1997, pp. 157–164.

[22] Cayson, S. and Berry, R., "Analysis of the flutter characteristics of the advanced kinetic energy missile (ADKEM) control surface," Tech. Rep. AD-A232377, Army Missile Command, Redstone Arsenal, AL. Guidance and Control Directorate, 1990.

[23] Murray, T., Gaphardt, M., and Stofko, D., "Modelling of flutter-induced limit cycles in a hydraulic fin servo with nonlinearities," AIAA PAPER 75-103, Jan 1975.

[24] Bae, J. and Lee, I., "Limit cycle oscillation of missile control fin with structural non-linearity," *Journal of Sound and Vibration*, Vol. 269, No. 3-5, Jan 2004, pp. 669–687.

[25] Matejka, D. Q., "Aeroelastic Bending of a Sounding Rocket Vehicles," *AIAA 2nd Sounding Rocket Technology Conference*, Dec. 1970, AIAA Paper 70-1400.

[26] Elyada, D., "Closed-Form Approach to Rocket-Vehicles Aeroelastic Divergence," *Journal of Spacecraft*, Vol. 26, No. 2, Mar.-Apr. 1989, pp. 95 – 102.

[27] Nakano, A., "The Effects of Malalignment on the Aeroelastic Behavior of Unguided Rockets," *Institute of Space and Aeronautical Science, University of Tokyo*, Vol. 33, No. 421, Feb 1968, pp. 73–96.

[28] Crimi, P., "Aeroelastic Stability and Response of Flexible Tactical Weapons," *AIAA 22rd Aerospace Sciences Meeting*, Jan. 1984, AIAA Paper 84-0392.

[29] Platus, D. H., "Aeroelastic Stability of Slender, Spinning Missiles," *Journal of Guidance, Control, and Dynamics*, Vol. 15, No. 1, Jan.-Feb. 1992, pp. 144 – 151.

[30] Stearns, B., Hathaway, W., and Whyte, B., "Flexible Body Trajectory Simulation – Preliminary Report," Tech. Rep. ARROW-010-88, ARROW Tech Associates, 1988.

[31] Legner, H. H., Lo, E. Y., and Reinecke, W., "On the Trajectory of Hypersonic Projectiles Undergoing Geometry Changes," *Aerospace Sciences Meeting and Exhibit*, Reno, Nevada, Jan. 10 – 13, 1994, AIAA Paper 94-0719.

[32] Livshits, D. S., Yaniv, S., and Karpel, M., "Dynamic Stability of Free Flight Rockets," *Proceedings of the 37th Structures, Structural Dynamics and Materials Conference, Salt Lake City, Utah*, AIAA, Reston, Virginia, April 15 – 17, 1996, pp. 230 – 236, AIAA Paper 96-1344.

[33] Maloney, J. G., Shelton, T. A., and Underhill, D. A., "Structural Dynamic Properties Of Tactical Missile Joints – Phase I," Tech. Rep. CR-6-348-945-001, General Dynamics Inc., 1970.

[34] Mikhail, A. G., "In-flight flexure and spin lock-in for antitank kinetic energy projectiles," *Journal of Spacecraft and Rockets*, Vol. 33, No. 5, Sept.-Oct. 1996, pp. 41 – 51.

[35] Murphy, C. H. and Mermagen, W. H., "Flight Mechanics of An Elastic Symmetric Missile," Tech. Rep. ARL-TR-2255, Army Research Laboratory, 2000.

[36] Murphy, C. H. and Mermagen, W. H., "Flight Motion of A Continuously Elastic Finned Missile," Tech. Rep. ARL-TR-2754, Army Research Laboratory, 2002.

[37] Reis, G. E. and Sundberg, W. D., "Calculated Aeroelastic Bending of a Sounding Rocket Based on Flight data," *Journal of Spacecraft*, Vol. 4, No. 11, Nov. 1967, pp. 1489–1494.

[38] Cochran, J. E. J. and Christensen, D. E., "Post-Launch Effects of Transverse Bending of a Spinning Free-Flight Rocket During the Guidance Phase," AIAA Paper 79-1668, 1979.

[39] Nasuti, F. and Innocenti, M., "Missile Trajectory Optimization With Agility Issues," *AIAA, Guidance, Navigation and Control Conference, San Diego, California*, July 29 – 31, 1996, AIAA Paper 96-3730.

[40] Muzumdar, D. and Hull, D. G., "Midcourse Guidance for a Short-Range Attack Missile Using Error Compensation," *Journal of Spacecraft and Rockets*, Vol. 33, No. 2, March-April 1996, pp. 191 – 197.

[41] Wang, Q., Lin, C. F., and D'Souza, C. N., "Optimality-Based Midcourse Guidance," *AIAA Guidance, Navigation and Control Conference, Monterey, California, Part 3*, Aug. 9 – 11, 1993, pp. 1734 – 1737, AIAA Paper 93-3893.

[42] Hallman, W. P., "Sensitivity Analysis For Trajectory Optimization Problems," *28th AIAA Aerospace Sciences Meeting, Reno, Nevada*, Jan. 8 – 11, 1990, AIAA Paper 90-0471.

[43] Han, D. and Balakrishnan, S. N., "Robust Adaptive Critic Based Neural Networks For Speed-Constrained Agile Missile Control," *AIAA Guidance, Navigation, and Control Conference and Exhibit, Portland, Oregon*, Aug. 9 – 11, 1999, pp. 640 – 650, AIAA Paper 99-4064.

[44] Imado, F., Kuroda, T., and Miwa, S., "Optimal Midcourse Guidance for Medium-Range Air-to-Air Missiles," *Journal of Guidance, Control, and Dynamics*, Vol. 13, No. 4, July-August 1990, pp. 603 – 608.

[45] Goland, M., "The Flutter of a Uniform Cantilever Wing," *Journal of Applied Mechanics*, Vol. 12, No. 4, December 1945, pp. A197 – A208.

[46] Fung, Y. C., *An introduction to the theory of aeroelasticity*, Wiley, New York, 1955.

[47] Bisplinghoff, R. L., Ashley, H., and Halfman, R. L., *Aeroelasticity*, Addison-Wesley Publishing Co., Reading, Massachusetts, 1955.

[48] Beck, M., "Die Knicklast des einseitig eingespannten, tangential gedrückten Stabes," *ZAMP*, Vol. 3, 1952, pp. 225 – 288.

[49] Bolotin, V. V., *Nonconservative Problems of the Theory of Elastic Stability*, Pergamon Press, New York, 1963.

[50] Leipholz, H. H. E., *Stability of elastic systems*, Sijthoff & Noordhoff, Alphen aan den Rijn, Netherlands, 1980.

[51] Chen, L.-W. and Ku, D.-M., "Eigenvalue Sensitivity in the Stability Analysis of Beck's Column with a Concentrated Mass at the Free End," *Journal of Sound and Vibration*, Vol. 153, No. 3, March 1992, pp. 403 – 411.

[52] Higuchi, K., "An Experimental model of a Flexible free-free column in Dynamic instability due to an End thrust Pt. 4 (A94-23876 06-39), Washington, DC, American Institute of Aeronautics and Astronautics, 1994, p. 2402-2408." *35th AIAA/ASME/ASCE/AHS/ASC Structures, Structural Dynamics, and Materials Conference, Hilton Head, South Carolina*, Apr. 18 – 20, 1994, pp. 2402 – 2408.

[53] Como, M., "Lateral Buckling of a Cantilever Subjected to a Transverse Follower Force," *International Journal of Solids and Structures*, Vol. 2, 1966, pp. 515 – 523.

[54] Wohlhart, K., "Dynamische Kippstabilität eines Plattenstreifens unter Folgelast," *Zeitschrift für Flugwissenschaften*, Vol. 19, No. 7, 1971, pp. 291 – 298.

[55] Feldt, W. T. and Herrmann, G., "Bending-Torsional Flutter of a Cantilevered Wing Containing a Tip Mass and Subjected to a Transverse Follower Force," *Journal of the Franklin Institute*, Vol. 297, No. 6, 1974, pp. 467 – 478.

[56] Huseyin, K., *Vibrations and Stability of Multiple Parameter Systems*, Sijthoff & Noordhoff International Publishers, Alphen aan den Rijn, The Netherlands, 1978.

[57] Livshits, D. and Yaniv, S., "Coupled Aeroelastic Analysis of a Free Flight Rocket," *MSC 1999 Aerospace Users' Conference Proceedings*, MSC Software, Santa Ana, CA, March 1999, pp. 1–11.

[58] Hodges, D. H., "A Mixed Variational Formulation Based on Exact Intrinsic Equations for Dynamics of Moving Beams," *International Journal of Solids and Structures*, Vol. 26, No. 11, 1990, pp. 1253 – 1273.

[59] Moore, F. G., McInnville, R. M., and Hymer, T., "The 1998 Vesion of The NSWC Aeroprediction Code: Part I – Summary Of New Theoretical Methodology," Tech. Rep. TR-98/1, NSWCDD, April 1998.

[60] Nielsen, J. N., *Missile Aerodynamics*, Nielsen Engineering and Research, Inc., Mountain View, California, 1988.

[61] Moore, F. G., *Approximate Methods For Weapon Aerodynamics*, American Institute of Aeronautics and Astronautics, Inc., Danvers, Massachusetts, 2000.

[62] Allen, H. J. and Perkins, E. W., "Characteristics of Flow over Inclined Bodies of Revolution," Tech. Rep. RM A50L07, NACA, 1951.

[63] Adams, M. C. and Sears, W. R., "Slender Body Theory – Review and Extension," *I. A. S. Annual Summer Meeting*, July 16 – 18, 1952.

[64] Allen, H. J., "Estimation of The Forces and Moments Acting on Inclined Bodies of Revolution," Tech. Rep. RM A9I26, NACA, 1949.

[65] Lighthill, M. J., "Oscillating Airfoils at High Mach Number," *Journal of The Aeronautical Sciences*, Vol. 20, June 1953, pp. 402 – 406.

[66] Lordon, J., Fare, J., and Pagan, D., "Supersonic Vortex Flows Around A Missile Body: Basic Experiment And Euler Numerical Computation," *Proceedings of NATO Symposium on Fluid Dynamics, Fluid Dynamics Panel, Advisory Group for Aerospace Research and Development, Friedrichshafen, Germany*, North Atlantic Treaty Organization, 1990, pp. 15:1–15:17.

[67] Chin, S. S., *Missile Configuration Design*, McGraw-Hill Book Company, Inc., 1961.

[68] Van Driest, E. R., "Turbulent Boundary Layers in Compressible Fluids," *Journal of Aeronautical Sciences*, Vol. 18, No. 3, March 1951, pp. 145 – 160.

[69] Moore, F. G., McInville, R. M., and Hymer, T. C., "The 1995 Version of the NSWC Aeroprediction Code: Part I – Summary of New Theoretical Methodology," Tech. Rep. NSWCDD/TR-94/379, Vol.1, 1995.

[70] De Jarnette, F. R., Ford, C. P., and Young, D. E., "Calculation of Pressures on Bodies at Low Angles of Attack in Supersonic Flow," *AIAA Journal*, Vol. 17, June 1979, pp. 529–536.

[71] Jumper, G. Y., Frushon, C. J., Longstreth, R. K., Smith, J., Willett, J., and Curtis, D., "Effects of Magnus Moments on Missile Aerodynamic Performance," Tech. Rep. PL-TR-92-2168 IP, No. 344, Philips Laboratory, Directorate of Geophysics, Air Force Systems Command, 1991.

[72] Mendenhall, M. R., *Tactical Missile Aerodynamics: Prediction Methodology*, Tht American Institute of Aeronautics and Astronautics, Inc., Washington DC, May 1991.

[73] Bithell, R. A. and Stoner, R. C., "Rapid Approach for Missile Synthesis, Rocket Synthesis Handbook," Tech. Rep. AFWAL-TR-81-3022, Vol.1, 1982.

[74] Hodges, D. H., "Lateral-Torsional Flutter of a Deep Cantilever Loaded by a Lateral Follower Force at the Tip," *Journal of Sound and Vibration*, Vol. 247, No. 1, Oct. 11, 2001, pp. 175 – 183.

[75] Hodges, D. H., Patil, M. J., and Chae, S., "Effect of Thrust on Bending-Torsion Flutter of Wings," *Journal of Aircraft*, Vol. 39, No. 2, Mar.-Apr. 2002, pp. 371 – 376.

[76] Patil, M. J., Hodges, D. H., and Cesnik, C. E. S., "Nonlinear Aeroelastic Analysis of Complete Aircraft in Subsonic Flow," *Journal of Aircraft*, Vol. 37, No. 5, Sept.-Oct. 2000, pp. 753 – 760.

[77] Peters, D. A., Karunamoorthy, S., and Cao, W.-M., "Finite State Induced Flow Models; Part I: Two-Dimensional Thin Airfoil," *Journal of Aircraft*, Vol. 32, No. 2, Mar.-Apr. 1995, pp. 313 – 322.

[78] Herrmann, G. and Jong, I.-C., "On the Destabilizing Effect of Damping in Nonconservative Elastic Systems," *Journal of Applied Mechanics*, Vol. 32, No. 3, September 1965, pp. 592 – 597.

[79] Anderson, J. D., *Introduction to Flight*, McGraw-Hill Book Company, New York, 2nd ed., 1985.

VITA

Seungmook Chae was born in Sunchon, South Korea, on Aug. 19, 1973. He received his Bachelor's degree in Aerospace Engineering in 1998 from Inha University, Inchon, South Korea. He came to the United States in August 1999 and joined the School of Aerospace Engineering at the Georgia Institute of Technology, where he received a Master of Science degree in Aerospace Engineering in December of 2000 and began a Ph.D. in 2001. Most of the work done during his study at Georgia Tech is presented here for the requirement of Doctor of Philosophy in Aerospace Engineering.